ARTICLE

doi:10.1038/nature24482

Visualization of chemical modifications in the human 80S ribosome structure

S. Kundhavai Natchiar[1,2,3,4,5]*, Alexander G. Myasnikov[1,2,3,4,5]*, Hanna Kratzat[1,2,3,4,5]†, Isabelle Hazemann[1,2,3,4,5] & Bruno P. Klaholz[1,2,3,4,5]

Chemical modifications of human ribosomal RNA (rRNA) are introduced during biogenesis and have been implicated in the dysregulation of protein synthesis, as is found in cancer and other diseases. However, their role in this phenomenon is unknown. Here we visualize more than 130 individual rRNA modifications in the three-dimensional structure of the human ribosome, explaining their structural and functional roles. In addition to a small number of universally conserved sites, we identify many eukaryote- or human-specific modifications and unique sites that form an extended shell in comparison to bacterial ribosomes, and which stabilize the RNA. Several of the modifications are associated with the binding sites of three ribosome-targeting antibiotics, or are associated with degenerate states in cancer, such as keto alkylations on nucleotide bases reminiscent of specialized ribosomes. This high-resolution structure of the human 80S ribosome paves the way towards understanding the role of epigenetic rRNA modifications in human diseases and suggests new possibilities for designing selective inhibitors and therapeutic drugs.

Human ribosomes are complex cellular machines that catalyse protein biosynthesis and contain 80 ribosomal proteins and four rRNA chains (28S, 5S and 5.8S rRNAs in the 60S subunit, and 18S rRNA in the 40S subunit)[1]. Human rRNAs carry numerous post-transcriptional modifications, such as methylations on ribose moieties and at different positions on the heterocyclic bases of A, G, C and U nucleotides that are introduced enzymatically during ribosome biogenesis, but the role of these modifications is essentially unknown. Many chemical modifications of human rRNAs have been reported. Around 95% of these modifications are 2′-OH ribose methylations (2′-O-Me) and conversions of U to pseudouridine (Ψ), whereas around 5% of modifications are predicted (i.e. found in databases) to contain methylated bases and other modifications[2–8]. Bacterial rRNAs contain a much smaller number of chemical modifications. Epigenetic rRNA modifications are thought to play an important role in catalytic activity as well as in RNA folding and stability[9–12], and they appear to modulate the activity of antibiotics[13,14], suggesting that they may influence the mode of interaction with drugs or lead to antibiotic resistance[15,16]. Some rRNA modifications are associated with dysregulated protein synthesis, including in cancer, inherited human disorders and other diseases[17–22], but the molecular basis of these phenomena remains unknown.

We have previously determined the structure of the human 80S ribosome at an average resolution of 3.6 Å, which has provided insights into the positions of amino-acid side chains and nucleotide bases[23] and made it possible to study a ligand complex of the human ribosome with an antibiotic[24]. However, at this resolution, it was not possible to address atomic details such as precise side chain conformations or small chemical modifications of the rRNA nucleotides, which were instead modelled as regular RNA nucleotides. Recently, rRNA modifications have been observed in the structures of bacterial and eukaryotic parasite ribosomes[25–27], but they have never been visualized in human ribosomes. Mapping predicted sites on the human ribosome structure would provide only incomplete information regarding both the presence of a site and its three-dimensional (3D) environment in the structure. Directly localizing and visualizing chemical modifications in the human ribosome structure would constitute a major advance, and could contribute to the development of new drugs. Therefore, we set out to determine the structure of the human ribosome to the highest possible resolution and to address the 3D localization and structural implications of rRNA modification sites. To investigate the potential role of rRNA modifications in drug specificity, we also determined the structure of the human ribosome in a complex with three inhibitors.

Features of the structure of the human ribosome

The structure of the human 80S ribosome was determined by single particle cryo-electron microscopy (cryo-EM) and refined using focused refinement[28] of the 60S ribosomal subunit and the 40S head and body parts during image processing (resolved to 2.9, 3.0 and 3.1 Å average resolution, respectively; see Methods; Fig. 1a, Extended Data Figs 1 and 2, and Extended Data Table 1a). Although only a few flexible peripheral regions are limited to a resolution of more than 3.5 Å, many regions have a local resolution of approximately 2.5 Å (Extended Data Fig. 2) consistent with the features resolved in the cryo-EM map (Fig. 1b, Extended Data Fig. 3). The present structure provides an unprecedented level of detail, even in the less ordered parts of the complex, including the 40S subunit (see Methods; Extended Data Fig. 3). Notably, the identities of nucleotide bases (and thus the RNA sequence in these regions) can now be determined unambiguously from the cryo-EM map, allowing stretches of incorrectly annotated nucleotide sequences in previous porcine and human ribosome structures[23,29] to be corrected (including rRNA sequence register shifts; see Methods; Fig. 1c, Extended Data Fig. 4) or reclassified from rRNA to protein (Fig. 1d, Extended Data Fig. 5a–c). Moreover, the structure reveals features that are usually not amenable to cryo-EM, such as alternative conformations of side chains and some amino acid modifications (see Methods; Fig. 1b, Extended Data Fig. 5d). Notably, this cryo-EM structure resolves many fine details of chemical modifications in the rRNA (see Methods for their identification; Extended Data Figs 5–10) as described below.

[1]Centre for Integrative Biology (CBI), Department of Integrated Structural Biology, IGBMC, CNRS, Inserm, Université de Strasbourg, 1 rue Laurent Fries, 67404 Illkirch, France. [2]Institute of Genetics and of Molecular and Cellular Biology (IGBMC), 1 rue Laurent Fries, Illkirch, France. [3]Centre National de la Recherche Scientifique (CNRS), UMR 7104, Illkirch, France. [4]Institut National de la Santé et de la Recherche Médicale (Inserm), U964, Illkirch, France. [5]Université de Strasbourg, Illkirch, France. †Present address: Gene Center, Ludwig-Maximilians-Universität, Munich, Germany.
*These authors contributed equally to this work.

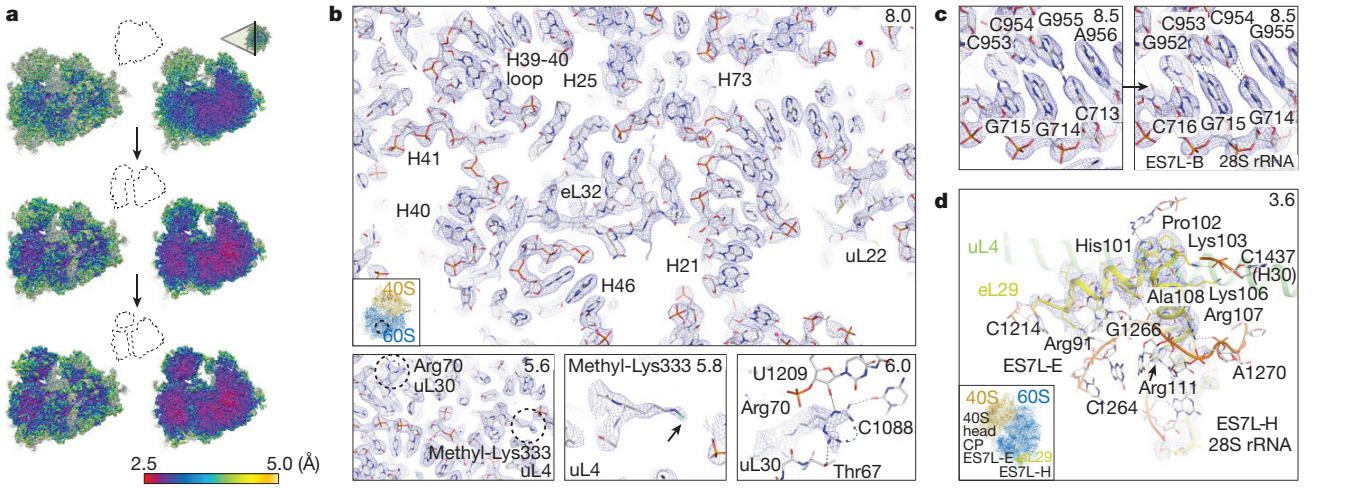

Figure 1 | High-resolution structure of the human 80S ribosome. a, Focused refinement of the human 80S structure refined first globally, then separately for the 40S and 60S ribosomal subunits and finally for the individual 40S body, 40S head and 60S regions (see also Extended Data Figs 1 and 2 and Extended Data Table 1a). **b**, A representative region illustrating the quality of the map and the high-resolution structural features; see also Extended Data Fig. 3. The map visualizes protein methylations and several dual conformations (lower panels; see also Extended Data Fig. 5 and Methods). Numbers in the corners indicate the local root mean square deviation contour level of the cryo-EM map (see Methods). **c**, An example of RNA register shift correction (left, cryo-EM map and partially refined previous atomic model; right, final atomic model; see also Extended Data Fig. 4). **d**, Reassignment of an RNA-annotated region into the C-terminal region of large ribosomal subunit protein eL29; see also Extended Data Fig. 5.

Localization and classification of rRNA modifications

Almost all the rRNA modifications are located in the 18S and 28S rRNAs, whereas none were seen in the 5S rRNA (where none were predicted). Two of the four modifications predicted to be present in the 5.8S rRNA were not seen (Gm75 was absent, but sub-stoichiometric methylation of Um14 cannot be ruled out; Extended Data Fig. 5e–h), and the other two predicted modifications (Ψ55 and Ψ69) were U isomers, which cannot be confirmed in the structure unless they form a specific hydrogen bond with the N1 position. Most of the modifications that we found are clustered around the inward-facing parts of the structure (Figs 2a and 3a). There are chemical modifications on many 2′-OH groups on ribose moieties and in precise but variable positions around the purine and pyrimidine rings of certain nucleotides (Figs 2 and 3; Extended Data Figs 7, 8 and 10). Some modifications were found in the predicted nucleotide positions[3,4,30], but many additional modifications were found on unpredicted sites. In total, we identified 136 rRNA modification sites in the entire structure, including 60 2′-O methylations (50 of which were among the 103 predicted sites and ten in unpredicted sites), 25 Ψ sites (out of 96 predicted Ψ sites; Ψs at the 71 remaining predicted Ψ sites cannot be confirmed structurally owing to the isomeric nature of this modification—Ψs are recognizable by their distinct hydrogen-bond pattern; Figs 2d and 3f) and 51 other base modifications (nine of which are at predicted sites and 42 are unpredicted). On the basis of this analysis we classified the modification sites as universally conserved locations (class I, 11 sites), human or eukaryote-specific modifications (class II, 73 sites), and new non-predicted unique sites (class III, 52 sites) (Extended Data Table 1b), some of which we discuss below to highlight their structural roles (Figs 2 and 3; a detailed list is provided in Extended Data Figs 6–10).

Class I rRNA modifications

The universally conserved rRNA modification sites (class I) cluster in functional centres such as the peptidyl transferase centre (PTC), the decoding centre, the mRNA and tRNA binding sites, the peptide exit tunnel (PET) and the ribosomal subunit interface. The recently reported *Escherichia coli* and *Thermus thermophilus* ribosome structures[25,26] contain 35 and 33 rRNA modification sites, respectively. We found modifications in only 11 of the equivalent nucleotide positions in the human ribosome (Supplementary Table 1). The types of chemical modification are conserved at these eleven sites (with the exception of G4550, see Methods). For example, the modifications $m^6{}_2$A1850 and $m^6{}_2$A1851 (18S rRNA) in the decoding centre of the 40S ribosomal subunit (Fig. 3d) are evolutionarily conserved dimethylations that are required for ribosome assembly[31]. The tip of H69 in the 60S ribosomal subunit is decorated with two universally conserved Ψs, m^3Ψ3762 and Ψ3764, the former being involved in bridge B2a.

Class II rRNA modifications

Class II comprises 73 human-specific modifications, predominantly 2′-O methylations and pseudouridylations that are also located at functional sites of the ribosome (Supplementary Table 2). For example, the bulge loop in H37 located next to the aminoacyl (A)-site finger contains two Ψs (Ψ1677 and Ψ1683), which are important for maintaining the translation reading frame[32]. There are four eukaryote-specific Ψs (Ψ4403, Ψ4442, Ψ4457 and Ψ4500; Fig. 2d) at the PTC; Ψ4500 is located on helix H92, which during translation would be close to the CCA end of an A-site tRNA, and m^3C4530 and Ψ4531 mark the peptidyl (P) tRNA binding site and could influence peptide formation. A 2′-O-Me triplet that is conserved in eukaryotes, comprising Am2363, Gm2364 and Cm2365, is lined up in the nearby H26–H47 junction, which interacts with and stabilizes the helix H73 bulge loop at the PET (Fig. 2e). Aromatic π-interactions with methylated sites, such as the one between the methyl groups in m^5C3782 (Fig. 2g) and Cm4536, introduce π-interactions with C3781 and Am3785 (which is involved in a kink turn), respectively, that jointly stabilize the H69–H71 loop. Finally, at the decoding centre, there are three modified nucleotides next to the substrate binding sites: Cm1703 in the mRNA channel, Ψ1243 above the A site and the predicted m^1acp^{3}Ψ1248 in the P site (Fig. 3e). Aminocarboxypropyl (acp) is one of the most chemically complex modifications in eukaryotic rRNA; the absence of hypermodification of m^1acp^{3}Ψ1248 strongly delays the maturation of 18S rRNA, and blocking all three modifications at the decoding centre simultaneously results in defective amino acid incorporation and neomycin resistance[33,34]. These examples show that the numerous human-specific modifications work together to preserve the topology of the functional sites. As several of these human-specific modifications are also found in yeast (Supplementary Table 2), this concept is likely to apply to eukaryotes in general.

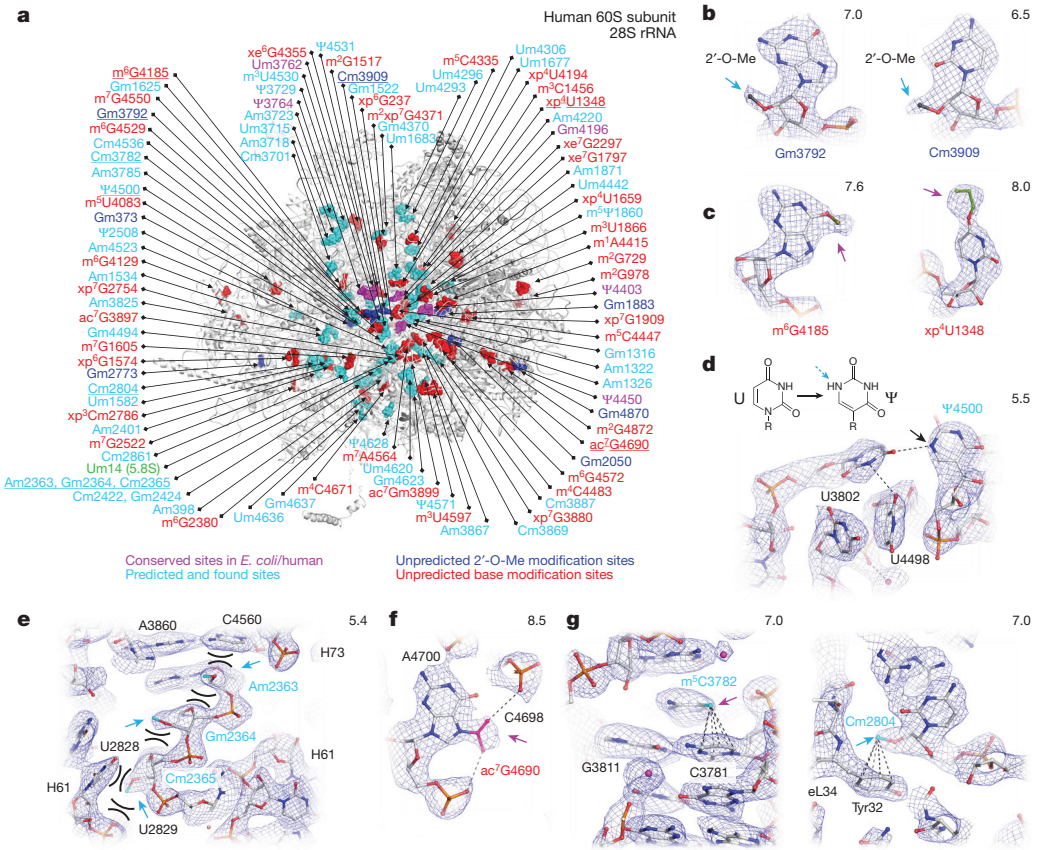

Figure 2 | Chemical modifications of the rRNA in the human 60S ribosomal subunit. a, Annotation of modified nucleotides on the human 28S rRNA; underlined nucleotides are those shown in **b**–**g**; see also Extended Data Figs 6–8. **b**, Examples of 2′-O-ribose methylations (cyan arrows throughout all figures; other modifications are indicated with magenta arrows). **c**, Examples of O6 and O4 methylations. **d**, Example of a pseudouridine (Ψ) with the characteristic hydrogen bonding in the N1 position. **e**, Example of a conserved 2′-O-ribose methylated nucleotide triplet and its van der Waals contacts (black arcs). **f**, A typical nucleotide, showing an unpredicted chemical modification that provides additional opportunities for RNA interactions. **g**, Examples of chemical modifications involving π-interactions with aromatic nucleotide bases (left) or amino-acid side chains (right).

Class III rRNA modifications

The class III sites comprise 52 unpredicted unique sites, including ten 2′-O-methylated nucleotides and 42 base-modified nucleotides in the 18S and 28S rRNAs (Supplementary Table 3). The base modifications include several unexpected chemical modification types that have not been reported previously. For example, G3897, Gm3899 and G4690 appear to be acetylated in the N7 position (Fig. 2f and Extended Data Figs 7 and 8) and form a network of modified nucleotides in the PTC and PET that stabilizes helices H72 and H73, suggesting possible involvement in translation. Similarly, the strong additional densities at the N7 positions in G1909, G1797, G3880 and G4371 are likely to correspond to hydrophilic moieties such as acetyl, acp or larger unidentified groups (annotated as 'xp'; Supplementary Table 3, Fig. 2c, f and Extended Data Figs 7, 8 and 10), but the precise chemical nature of these substituents remains to be identified. In 18S rRNA, we found two cytosine acetylations that are not found in databases but are universally conserved[5,35,36] (ac^4C1337 and ac^4C1842; Fig. 3b and Extended Data Fig. 10). ac^4C1842, whose acetylation is crucial for 40S subunit biogenesis[35], contributes to the inter-subunit bridge eB14. A series of nucleotides that are modified at the oxygen position (such as O6 in G and O4 in U) are of particular note, as this is an unusual modification in RNA (see Methods; Fig. 2c and Extended Data Fig. 8).

rRNA modifications in inhibitor binding pockets

Because rRNA modifications appear to influence the activity and specificity of antibiotics[13–16], we determined the structure of the human ribosome with three simultaneously bound inhibitors, including two eukaryote-specific antibiotics (see Methods). Inspection of the ligand pockets shows that the inhibitors are either in direct contact with or in very close proximity to rRNA modification sites (Fig. 4). Indeed, the 2′-O-Me group of Cm3909 (a human-specific modification) provides hydrophobic contacts to homoharringtonine (HHT) at the PTC, complemented by the nearby Ψ4530 and Ψ4531 (eukaryote and human-specific modifications, respectively; Fig. 4a). Bound hygromycin B (HYG) is not in direct contact with any rRNA modifications, but is in proximity to Cm1703 (human-specific), m^3U1830, m^6A1832, $m^6{}_2A1850$ and $m^6{}_2A1851$ (18S rRNA; Fig. 4b). The binding site of cycloheximide (CHX) is also interesting as CHX competes with the CCA end of the E-site tRNA. The extra methyl group of m^2xp^7G4371 generates a hydrophobic contact with CHX, which is also within drug-able distance of the 2′-O-methyl group of Gm4370 (Fig. 4c, d). In the non-inhibited state, the CCA end of the E-site tRNA interacts with the modified moieties of Gm4370 and m^2xp^7G4371 (Fig. 4c). Several other known inhibitor binding pockets also contain modified nucleotides (see Methods). Together, these observations suggest that rRNA modifications have a role in the molecular recognition of inhibitors and of tRNAs in the A, P and E sites.

Structural and functional role of rRNA modifications

This study provides, to our knowledge, the highest resolution structure and the most complete atomic model of the human ribosome to date, including the visualization of more than 130 chemical modifications of human rRNA introduced during biogenesis, many of which were not predicted from databases based on biochemical studies. Far beyond a

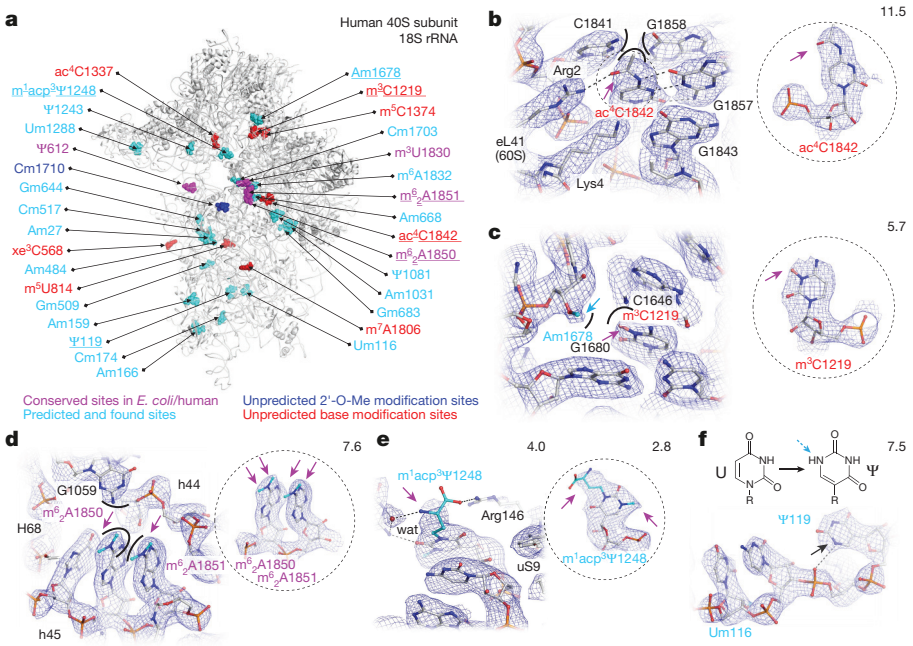

Figure 3 | Chemical modifications of rRNA in the human 40S ribosomal subunit. a, Annotation of modified nucleotides on the human 18S rRNA; underlined nucleotides are those shown in **b**–**f**; see also Extended Data Figs 9 and 10. **b**, Example of a cytosine acetylation providing additional hydrogen bonds (dotted lines) and van der Waals contacts (black arcs). **c**, Example of a contact between two modified nucleotides. **d**, Example of a pair of N6 adenine dimethylations in the decoding centre. **e**, A conserved hyper-modified site in the PTC involving a water molecule-mediated interaction. Right, full visualization of the two modifications at a lower map contour level. **f**, Example of Ψs with characteristic hydrogen bonding in the N1 position.

simple threading and mapping of predicted sites on an atomic model, the experimental visualization of these rRNA modifications allows us to investigate their individual 3D environments inside the human ribosome, and thereby provides unprecedented insights into their role. Two clear conclusions can be drawn from the present analysis. First, rRNA modifications have both local and collective roles in the stabilization of rRNA structure and in specific interactions that cannot be provided by regular nucleotides; and second, all inhibitor binding sites contain rRNA modifications in the first and/or second residue layers, which have not been accounted for in drug design. Notably, most modifications face other rRNA elements (complemented in part by ribosomal proteins) and only a few are located at the ribosome surface. The presence of rRNA modifications in the mature 80S ribosome has two possible explanations: (i) they are required for biogenesis of ribosome assembly and are simply left behind, or (ii) they have specific functions in the mature human ribosome, and some may be introduced specifically to acquire new specialized functions; we consider the second explanation to be more likely. Notably, essentially all chemical modifications of the human ribosome are located in bulges, interior and hairpin loops, and near the termini of RNA helices (Supplementary

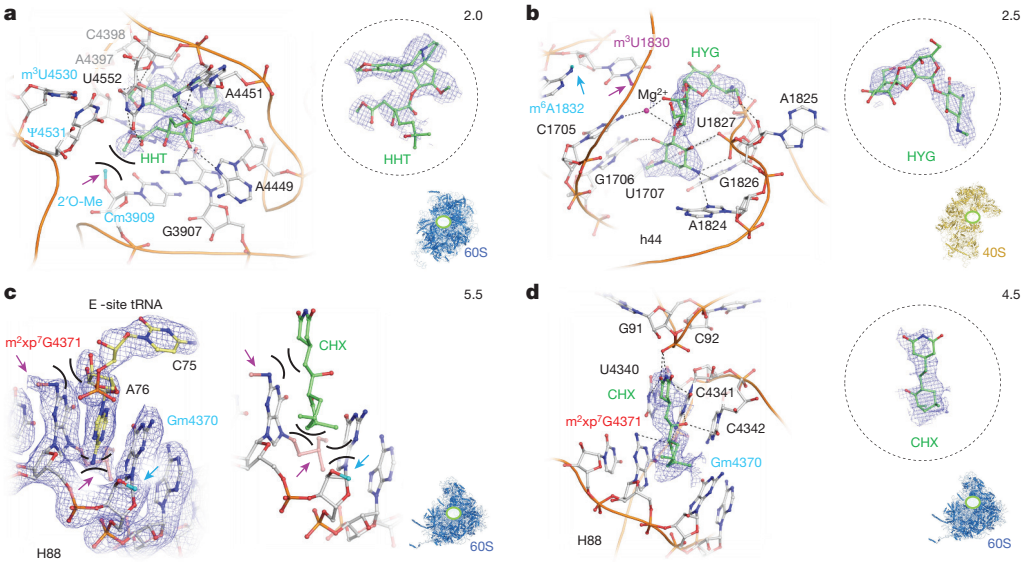

Figure 4 | Chemical modifications in the vicinity of ligand-binding pockets of the human 80S ribosome with three bound inhibitors. a, The HHT-binding site at the PTC (60S). **b**, The HYG-binding site (40S). **c**, The CHX-binding site (tRNA E-site). Right, model of CHX in the high-resolution 80S ribosome structure. **d**, CHX density in a subpopulation of the 80S complex (see Methods).

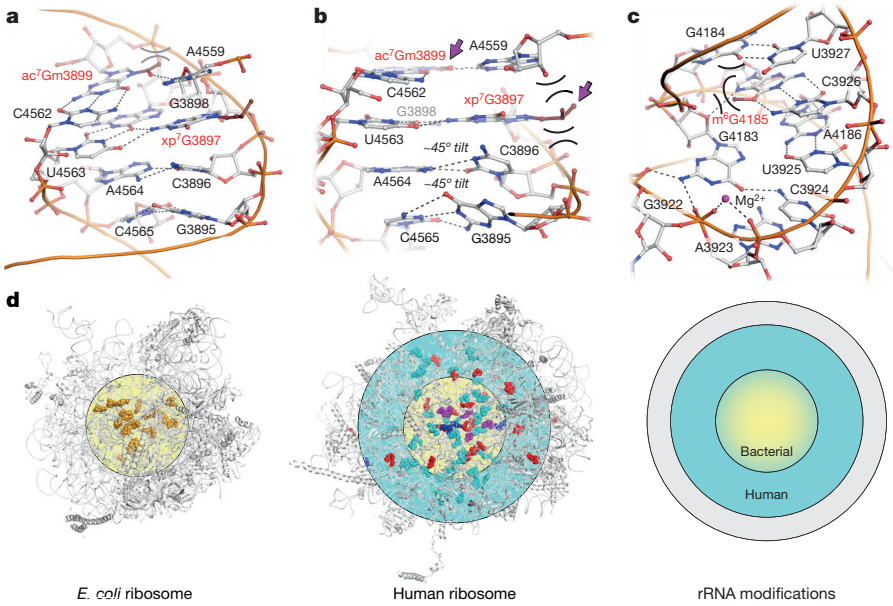

Figure 5 | Role of chemical modifications and their evolutionary extension between prokaryotic and eukaryotic species. a–c, Role in the stabilization of the rRNA structure. **d**, Comparison of modification sites in bacterial ribosomes (left) with those in the human ribosome (middle) reveals an evolutionarily extended additional shell of rRNA modifications (see also Extended Data Fig. 11).

Tables 1–3) involving special RNA structural elements including base triples, A-minor motifs, kink turns and flipped-out nucleotides. These regions tend to be more structurally flexible and benefit from stabilization through increased hydrogen-bonding possibilities (as in Figs 2d, f, 3b, e, f and Extended Data Figs 7, 8 and 10), additional π-stacking interactions with nucleotide bases or aromatic amino acid side chains (Fig. 2g), or van der Waals contacts between hydrophobic residues in the case of methylations and other alkylations (Figs 2b, c, e, 3b–d and Extended Data Figs 7, 8 and 10). A characteristic feature of the modifications is that they either stabilize unconventional base pairing, or perturb conventional base pairs (such as at the end of helices H86, H38 and h44), and thus induce base tilting (for example, xp^{7}G3880; Fig. 5a–c and Extended Data Fig. 8). Some modifications appear to favour wobble base pairing, like that seen in DNA[37,38], or base triple interactions, which can propagate to neighbour base pairs (Fig. 5a–c; see Methods). As a result, the concept of RNA stabilisation by 2′-O methylations[12,39] also applies to nucleotide base modifications, such as acetyl groups that create special nucleotide geometries and additional hydrogen bonding (for example, ac^{4}C1842; Fig. 3b; see Methods).

An extended shell of rRNA modifications in eukaryotes

The rRNA modifications examined here show that the majority of modifications occur in or close to functionally important sites. Though this was previously known to be true for bacterial ribosomes, which carry only a small number of modifications, the present work shows that this also applies to eukaryotic, and in particular, human ribosomes (Fig. 5d and Extended Data Fig. 11). However, the complexity of modifications increases from prokaryotic to eukaryotic species, suggesting that humans (Fig. 5d), and other eukaryotes such as yeast (Supplementary Table 2), have evolved an extended additional shell of rRNA modifications around the functional centres. This additional complexity parallels the evolutionary shift towards eukaryotic ribosomal RNAs and proteins[40], and suggests that epigenetic rRNA modifications may have a role in fine-tuning the regulation of protein synthesis in eukaryotes, possibly by acting collectively as a 'cushion' around the functionally important regions. This regulation could be further modulated by specific rRNA modifications that differ between healthy and dysregulated states. This is illustrated by the presence of 12 unpredicted sites that contain modifications of guanosine and uridine in their O6 and O4 keto groups, respectively, which are otherwise rarely seen in RNA (Fig. 2c and Extended Data Fig. 8; Supplementary Table 3) and never seen in bacteria[25,26]. These modifications are reminiscent of DNA alkylations that occur in the context of cancer and correlate with translation defects[41] and increased mutagenicity[42,43]. While these modifications were unexpected, their presence in the HeLa cells used in our study may indicate that ribosomes are modified differently in different cell types.

Outlook

In summary, this work visualizes chemical modifications of rRNA in the human ribosome that are introduced during biogenesis and maturation and highlights their structural and functional roles within their 3D molecular environment (see also Supplementary Video). The atomic model of the human ribosome that we describe provides an extensive repertoire of rRNA modifications, including many new rRNA modification sites that might enable the design of new functional assays. Our structural analysis of rRNA with three simultaneously bound inhibitors suggests the presence of specific modification sites that could be targeted for selective ligand interactions. This concept could provide a basis for disease-specific drug developments that exploit the altered reactivity and interactions of specifically modified rRNA residues, notably in the context of human-specific inhibitors against protein synthesis dysregulations, such as those seen in cancer[19,24,44], genetic diseases or diseases related to ribosome biogenesis[45]. This study underlines the importance of considering rRNA modifications for future structure-based drug design, both in humans and in bacteria, which could also benefit from synergistic effects between simultaneously bound inhibitors.

Finally, the presence of many unpredicted rRNA modification sites and the absence of some of the expected 2′-O-Me sites suggest that chemical rRNA modifications in human ribosomes may differ between cell types, such as between normal cells and cancer cells (such as the HeLa cells used here). For instance, some of the class III rRNA modifications could be a signature of cancerous states. This suggests that it might be possible to distinguish between differently specialized ribosomes. Consistent with recent evidence that modifications could be sub-stoichiometric (see also Extended Data Fig. 5e) and ribosome-specific[22,46–50], this extends the concept of ribosome heterogeneity to the level of rRNA modifications at specific sites with potential implications for human health.

Online Content Methods, along with any additional Extended Data display items and Source Data, are available in the online version of the paper; references unique to these sections appear only in the online paper.

Received 27 June; accepted 3 October 2017.
Published online 15 November 2017.

1. Rodnina, M. V., Fischer, N., Maracci, C. & Stark, H. Ribosome dynamics during decoding. *Phil. Trans. R. Soc. Lond. B* **372,** 1716 (2017).
2. Decatur, W. A. & Fournier, M. J. rRNA modifications and ribosome function. *Trends Biochem. Sci.* **27,** 344–351 (2002).
3. Cantara, W. A. *et al.* The RNA Modification Database, RNAMDB: 2011 update. *Nucleic Acids Res.* **39,** D195–D201 (2011).
4. Machnicka, M. A. *et al.* MODOMICS: a database of RNA modification pathways—2013 update. *Nucleic Acids Res.* **41,** D262–D267 (2013).
5. Sharma, S. & Lafontaine, D. L. J. 'View from a bridge': a new perspective on eukaryotic rRNA base modification. *Trends Biochem. Sci.* **40,** 560–575 (2015).
6. Maden, B. E. Identification of the locations of the methyl groups in 18 S ribosomal RNA from *Xenopus laevis* and man. *J. Mol. Biol.* **189,** 681–699 (1986).
7. Maden, B. E. Locations of methyl groups in 28 S rRNA of *Xenopus laevis* and man: clustering in the conserved core of molecule. *J. Mol. Biol.* **201,** 289–314 (1988).
8. Piekna-Przybylska, D., Decatur, W. A. & Fournier, M. J. The 3D rRNA modification maps database: with interactive tools for ribosome analysis. *Nucleic Acids Res.* **36,** D178–D183 (2008).
9. Baxter-Roshek, J. L., Petrov, A. N. & Dinman, J. D. Optimization of ribosome structure and function by rRNA base modification. *PLoS One* **2,** e174 (2007).
10. Ofengand, J. & Bakin, A. Mapping to nucleotide resolution of pseudouridine residues in large subunit ribosomal RNAs from representative eukaryotes, prokaryotes, archaebacteria, mitochondria and chloroplasts. *J. Mol. Biol.* **266,** 246–268 (1997).
11. Green, R. & Noller, H. F. In vitro complementation analysis localizes 23S rRNA posttranscriptional modifications that are required for *Escherichia coli* 50S ribosomal subunit assembly and function. *RNA* **2,** 1011–1021 (1996).
12. Auffinger, P. & Westhof, E. in *Effects of Pseudouridylation on tRNA Hydration and Dynamics: A Theoretical Approach in Modification and Editing of RNA* (eds Grosjean, H. & Benne, R.) 103–112 (ASM, 1998).
13. Long, K. S. & Vester, B. Resistance to linezolid caused by modifications at its binding site on the ribosome. *Antimicrob. Agents Chemother.* **56,** 603–612 (2012).
14. Benítez-Páez, A., Cárdenas-Brito, S., Corredor, M., Villarroya, M. & Armengod, M. E. Impairing methylations at ribosome RNA, a point mutation-dependent strategy for aminoglycoside resistance: the rsmG case. *Biomedica* **34** (Suppl. 1), 41–49 (2014).
15. Stojković, V., Noda-Garcia, L., Tawfik, D. S. & Fujimori, D. G. Antibiotic resistance evolved via inactivation of a ribosomal RNA methylating enzyme. *Nucleic Acids Res.* **44,** 8897–8907 (2016).
16. Wirmer, J. & Westhof, E. Molecular contacts between antibiotics and the 30S ribosomal particle. *Methods Enzymol.* **415,** 180–202 (2006).
17. Gonzales, B. *et al.* The Treacher Collins syndrome (TCOF1) gene product is involved in pre-rRNA methylation. *Hum. Mol. Genet.* **14,** 2035–2043 (2005).
18. Freed, E. F., Bleichert, F., Dutca, L. M. & Baserga, S. J. When ribosomes go bad: diseases of ribosome biogenesis. *Mol. Biosyst.* **6,** 481–493 (2010).
19. Penzo, M., Galbiati, A., Treré, D. & Montanaro, L. The importance of being (slightly) modified: the role of rRNA editing on gene expression control and its connections with cancer. *Biochim. Biophys. Acta* **1866,** 330–338 (2016).
20. Lafontaine, D. L. J. Noncoding RNAs in eukaryotic ribosome biogenesis and function. *Nat. Struct. Mol. Biol.* **22,** 11–19 (2015).
21. Bellodi, C. *et al.* H/ACA small RNA dysfunctions in disease reveal key roles for noncoding RNA modifications in hematopoietic stem cell differentiation. *Cell Reports* **3,** 1493–1502 (2013).
22. Sloan, K. E. *et al.* Tuning the ribosome: The influence of rRNA modification on eukaryotic ribosome biogenesis and function. *RNA Biol.* **2,** 1–16 (2016).
23. Khatter, H., Myasnikov, A. G., Natchiar, S. K. & Klaholz, B. P. Structure of the human 80S ribosome. *Nature* **520,** 640–645 (2015).
24. Myasnikov, A. G. *et al.* Structure–function insights reveal the human ribosome as a cancer target for antibiotics. *Nat. Commun.* **7,** 12856 (2016).
25. Fischer, N. *et al.* Structure of the *E. coli* ribosome–EF-Tu complex at <3 Å resolution by Cs-corrected cryo-EM. *Nature* **520,** 567–570 (2015).
26. Polikanov, Y. S., Melnikov, S. V., Söll, D. & Steitz, T. A. Structural insights into the role of rRNA modifications in protein synthesis and ribosome assembly. *Nat. Struct. Mol. Biol.* **22,** 342–344 (2015).
27. Shalev-Benami, M. *et al.* 2.8-Å cryo-EM structure of the large ribosomal subunit from the eukaryotic parasite *Leishmania*. *Cell Reports* **16,** 288–294 (2016).
28. von Loeffelholz, O. *et al.* Focused classification and refinement in high-resolution cryo-EM structural analysis of ribosome complexes. *Curr. Opin. Struct. Biol.* **46,** 140–148 (2017).
29. Voorhees, R. M., Fernández, I. S., Scheres, S. H. W. & Hegde, R. S. Structure of the mammalian ribosome–Sec61 complex to 3.4 Å resolution. *Cell* **157,** 1632–1643 (2014).
30. Limbach, P. A., Crain, P. F. & McCloskey, J. A. Summary: the modified nucleosides of RNA. *Nucleic Acids Res.* **22,** 2183–2196 (1994).
31. Zorbas, C. *et al.* The human 18S rRNA base methyltransferases DIMT1L and WBSCR22-TRMT112 but not rRNA modification are required for ribosome biogenesis. *Mol. Biol. Cell* **26,** 2080–2095 (2015).
32. Baudin-Baillieu, A. *et al.* Nucleotide modifications in three functionally important regions of the *Saccharomyces cerevisiae* ribosome affect translation accuracy. *Nucleic Acids Res.* **37,** 7665–7677 (2009).
33. Liang, X.-H., Liu, Q. & Fournier, M. J. Loss of rRNA modifications in the decoding center of the ribosome impairs translation and strongly delays pre-rRNA processing. *RNA* **15,** 1716–1728 (2009).
34. Meyer, B. *et al.* Ribosome biogenesis factor Tsr3 is the aminocarboxypropyl transferase responsible for 18S rRNA hypermodification in yeast and humans. *Nucleic Acids Res.* **44,** 4304–4316 (2016).
35. Ito, S. *et al.* A single acetylation of 18 S rRNA is essential for biogenesis of the small ribosomal subunit in *Saccharomyces cerevisiae*. *J. Biol. Chem.* **289,** 26201–26212 (2014).
36. Sharma, S. *et al.* Yeast Kre33 and human NAT10 are conserved 18S rRNA cytosine acetyltransferases that modify tRNAs assisted by the adaptor Tan1/THUMPD1. *Nucleic Acids Res.* **43,** 2242–2258 (2015).
37. Hermann, T. & Westhof, E. Non-Watson–Crick base pairs in RNA–protein recognition. *Chem. Biol.* **6,** R335–R343 (1999).
38. Swann, P. F. Why do O6-alkylguanine and O4-alkylthymine miscode? The relationship between the structure of DNA containing O6-alkylguanine and O4-alkylthymine and the mutagenic properties of these bases. *Mutat. Res.* **233,** 81–94 (1990).
39. Sergeeva, O. V., Bogdanov, A. A. & Sergiev, P. V. What do we know about ribosomal RNA methylation in *Escherichia coli*? *Biochimie* **117,** 110–118 (2015).
40. Melnikov, S. *et al.* One core, two shells: bacterial and eukaryotic ribosomes. *Nat. Struct. Mol. Biol.* **19,** 560–567 (2012).
41. Hudson, B. H. & Zaher, H. S. O6-Methylguanosine leads to position-dependent effects on ribosome speed and fidelity. *RNA* **21,** 1648–1659 (2015).
42. Roos, W. P., Thomas, A. D. & Kaina, B. DNA damage and the balance between survival and death in cancer biology. *Nat. Rev. Cancer* **16,** 20–33 (2016).
43. Herzig, M. C. S. *et al.* DNA alkylating agent protects against spontaneous hepatocellular carcinoma regardless of O6-methylguanine-DNA methyltransferase status. *Cancer Prev. Res. (Phila.)* **9,** 245–252 (2016).
44. Marcel, V. *et al.* p53 acts as a safeguard of translational control by regulating fibrillarin and rRNA methylation in cancer. *Cancer Cell* **24,** 318–330 (2013).
45. Farley, K. I. & Baserga, S. J. Probing the mechanisms underlying human diseases in making ribosomes. *Biochem. Soc. Trans.* **44,** 1035–1044 (2016).
46. Dinman, J. D. Pathways to specialized ribosomes: the Brussels lecture. *J. Mol. Biol.* **428** (10 Pt B), 2186–2194 (2016).
47. Slavov, N., Semrau, S., Airoldi, E., Budnik, B. & van Oudenaarden, A. Differential stoichiometry among core ribosomal proteins. *Cell Reports* **13,** 865–873 (2015).
48. Preiss, T. All ribosomes are created equal. Really? *Trends Biochem. Sci.* **41,** 121–123 (2016).
49. Marcel, V., Catez, F. & Diaz, J.-J. Ribosome heterogeneity in tumorigenesis: the rRNA point of view. *Mol. Cell. Oncol.* **2,** e983755 (2015).
50. Krogh, N. *et al.* Profiling of 2′-O-Me in human rRNA reveals a subset of fractionally modified positions and provides evidence for ribosome heterogeneity. *Nucleic Acids Res.* **44,** 7884–7895 (2016).

Supplementary Information is available in the online version of the paper.

Acknowledgements We thank J. Michalon, R. Fritz and R. David for IT support, J.-F. Ménétret for technical support, M.-C. Poterszman for constant support, the IGBMC cell culture facilities for HeLa cell production, and B. Beinsteiner for making the 3D animation. We thank D. Agard and S. Zheng for making MotionCor2 available ahead of publication. This work was supported by CNRS, Association pour la Recherche sur le Cancer (ARC), Institut National du Cancer (INCa), Ligue nationale contre le cancer (Ligue), Agence National pour la Recherche (ANR; ANR-10-LABX-0030-INRT under the program Investissements d'Avenir ANR-10-IDEX-0002-02). The electron microscope facility was supported by the Alsace Region, the Fondation pour la Recherche Médicale (FRM), Inserm, CNRS and ARC, by Instruct-ULTRA as part of the European Union's Horizon 2020 (grant ID 731005), the French Infrastructure for Integrated Structural Biology (FRISBI; ANR-10-INSB-05-01) and by Instruct-ERIC.

Author Contributions I.H. performed sample preparation, A.G.M. acquired cryo-EM data, A.G.M., H.K. and S.K.N. performed image processing, S.K.N. did structure refinement and model building, and S.K.N. and B.P.K. performed structural analysis of the rRNA. All authors analysed the data. B.P.K supervised the project and wrote the manuscript with input from all authors.

Author Information Reprints and permissions information is available at www.nature.com/reprints. The authors declare no competing financial interests. Readers are welcome to comment on the online version of the paper. Publisher's note: Springer Nature remains neutral with regard to jurisdictional claims in published maps and institutional affiliations. Correspondence and requests for materials should be addressed to B.P.K. (klaholz@igbmc.fr).

Reviewer Information *Nature* thanks J. D. Dinman and the other anonymous reviewer(s) for their contribution to the peer review of this work.

METHODS

Complex formation and cryo-EM data processing. Human 80S ribosomes were prepared from HeLa cells as described previously[51]. HeLa cells were tested by PCR and certified to be free of mycoplasma. Freshly prepared human 80S ribosomes (2.5 μl) were incubated for 2 h on ice with 10-fold molar excess of HHT, HYG and CHX (4-[(2*R*)-2-[(1*S*,3*S*,5*S*)-3,5-dimethyl-2-oxocyclohexyl]-2-hydroxyethyl] piperidine-2,6-dione). These ligands were selected because they bind to three different ribosomal sites, as observed in bacterial and yeast ribosomes[26,52–55]. HYG binds the decoding centre in the 40S subunit, HHT binds in the PTC and CHX binds in the tRNA E-site of the 60S subunit. Samples were diluted from 2 mg ml^{-1} to 0.5 mg ml^{-1} , applied to 300-mesh holey carbon Quantifoil 2/2 grids (Quantifoil Micro Tools) and flash-frozen as described[23]. To reduce preferential orientation effects and improve angular sampling, we used holey carbon grids both with and without a thin carbon layer. Data were collected on the in-house spherical aberration (Cs)-corrected Titan Krios S-FEG instrument (FEI) operating at an acceleration voltage of 300 kV and a nominal underfocus of $\Delta z = -0.4$ to -2.5 μm at a magnification of 77,778 (nominal pixel size of 0.9 Å). We recorded 6,528 movies using a back-thinned direct electron detector (Falcon II) 4,096 × 4,096 camera with dose fractionation (seven individual frames were collected, starting from the second one). Total exposure time was 1 s, with a dose of 60 e$^-$ Å^{-2} (or 3.5 e$^-$ Å^{-2} per frame). Images in the stack were aligned using the whole-image motion correction method using MotionCor2[56]. We used Gautomatch (http://www.mrc-lmb.cam.ac.uk/kzhang/Gautomatch/), to pick 398,104 particle boxes automatically, and the contrast transfer function of each image was determined using GCTF as a standalone program on the micrograph and particle levels[57]. For the first steps of image processing we used coarsened data binned by a factor of 4 (C4 images). First, we applied 2D classification to remove images with ice or other contaminants (253,374 particles left), followed by 3D classification to remove bad particles (181,546 good particles left). After 3D refinement, we performed an additional 3D classification (see workflow in Extended Data Fig. 1) to separate 80S ribosomes in rotated (43,312) and non-rotated (138,234 particles) states. Both complexes contain E-site tRNA and the rotated 80S particles contain the protein eEF2, whereas the non-rotated particles contain no factors and were refined further as a class of CHX-containing 80S particles (similarly to a procedure described previously[24]). To obtain the best possible resolution of the 80S ribosome, all particles of the non-rotated ribosome were used (138,234 particles), and a 3D refinement was performed using data with the original pixel size and a box size of 640 pixels. A further improved cryo-EM map was obtained by focused refinement[28] using individual masks, first around the 40S and 60S ribosomal subunits, and then on the individual 40S head, 40S body and 60S subunit regions (see also Extended Data Fig. 2), which allowed us to obtain a high-resolution map, including for the less well-ordered parts, such as the 40S ribosomal subunit (Extended Data Fig. 3). The binary masks were created with the 'relion_mask_create' tool using at least three pixels extension and seven pixels for smoothening of the edges. The post-processing procedure implemented in RELION 1.4[58] was applied to the final maps for appropriate masking, B-factor sharpening (−66.5, −70.6, −82.4 Å^2 for the 60S, 40S body and 40S head regions, respectively) and resolution estimation to avoid over-fitting[59]. Precise magnification calibration was done by fine-scaling of the cryo-EM map with respect to the previous atomic model[23,24]. The procedure consists of cross-correlation calculations between the cryo-EM map and a map calculated from the atomic model for varying scales by increments of 0.01 of the pixel size (in Chimera software), here in the range of 1.65–1.80 on the 2× coarsened data (nominal pixel size of 1.8 Å), with 1.70 Å being the optimal value; for the non-coarsened data this corresponds to a pixel size of 0.85 Å on the specimen level and a calibrated magnification of 82,353× (1.05882× the nominal magnification). The resolution was estimated in Relion at 0.143 FSC criterion[60], indicating an average resolution of 2.9, 3.0 and 3.1 Å for the 60S subunit, 40S body and 40S head, respectively (Extended Data Fig. 2). Local resolution estimation with the software ResMap[61] shows that many regions reach 2.5 Å resolution (Extended Data Fig. 2).

Atomic model building and refinement, and localization of rRNA modifications. The cryo-EM maps were interpreted using Chimera[62] and COOT[63] to derive an atomic model of the human ribosome obtained by model building and structure refinement[64] using Phenix[65]. Modified nucleotides and amino acids templates were drawn and the restraints for the atomic model fitting and refinements were generated using JLigand[66]. The atomic model of the human ribosome (PDB: 4UG0 and 5LKS)[23,24] was used as starting point and refined against the experimental cryo-EM map by iterative manual model building and restrained parameter-refinement protocols (real-space refinement, positional refinement, grouped B-factor refinement and simulated annealing as described[23,24]). This involved numerous register shift corrections (mostly +1 or −1) in the 28S rRNA regions 452–519, 655–759, 940–1000, 1060–1080, 1250–1294 and 3761–3773 at the periphery of the 60S subunit, which were rebuilt and refined (Extended Data Fig. 4). Typical rRNA sequence register shifts of −1 and +1 in the 28S rRNA at the periphery of the 60S subunit were rebuilt and refined (for example, helix H25 and helices A and B of expansion segment 7L (ES7L); Fig. 1c and Extended Data Fig. 4; interestingly, these three regions are particularly G/C rich). Other rebuilt or reassigned sections comprise 28S rRNA regions 1697–1709, 1833–1841 (+1 shift), 2077–2106, 2763–2768 (+1 shift), 4730–4776 (+1 shift), 4859–4895 (−1 shift) and 4925–4959, and 18S rRNA regions 311–339, 873–876 (+1 shift) and 1407–1438. Several of these corrections clarify the characteristic interaction pattern of flipped-out nucleotides (Extended Data Fig. 4). Moreover, a region interpreted as 28S rRNA (2114–2123) in previous human and porcine ribosome structures in fact corresponds to the 91–116 region of the large ribosomal subunit protein eL29, which could now be traced unambiguously, including side chains. eL29 forms two α-helices that bridge the rRNA region 1214 with regions 1240 and 1270 (28S rRNA regions ES7L-E, ES7L-H and helix H30, respectively, Fig. 1d; Extended Data Fig. 5a–c). In addition, this eL29 stretch packs against the long N-terminal helix of the uL30 protein through a series of hydrophobic contacts (Fig. 1d). These regions are involved in the architecture of the 60S subunit, notably in stabilizing the peripheral rRNA segment ES7L.

Chemical modifications were identified on the basis of the presence of significant additional densities in the 2′-OH position (indicated by cyan arrows in the figures) and on nucleotide bases. As the resolution is not constant throughout the map, all modifications were examined individually, taking into account local resolution features of the neighbouring residues (see representative examples in Extended Data Fig. 5i, j, in which the presence and absence of modifications are compared). The map contour level was adjusted individually, including for the regions comprising the inhibitors, which are not fully stoichiometrically bound. For the contour level of the cryo-EM map, numbers in the figure corners indicate the local root mean square deviation from the mean (similar to sigma levels). Annotated residues were cross-checked for predictive presence or absence in databases[32] such as the RNA Modification Database (mods.rna.albany.edu[3,30]) and the modification patterns listed in MODOMICS[4]. New chemical groups were annotated on the basis of size, shape and hydrogen-bonding potential with neighbour residues. For example, G3897, Gm3899 and G4690 appear to be acetylated at the N7 position, on the basis of the additional density being in plane with the nucleotide base and the hydrogen-bond patterns with neighbouring phosphate groups (Fig. 2f and Extended Data Fig. 8). Annotations of the chemical nature of modifications are reliable throughout (methyl (m), acetyl (ac), and so on), with the exception of larger moieties such as propyl and other similar alkyl groups (for example, new 'xp' sites), which cannot be distinguished and remain to be characterized with respect to their chemical nature. Chemical modifications of amino acids include methylations of Lys333 (protein uL4) and Lys98 (eL40; Extended Data Fig. 5d). The fact that the RNA helicase II/Guα interacts with the 264–333 region of uL4 during 28S rRNA maturation[67] suggests that this unpredicted Lys333 modification is involved in ribosome biogenesis.

The final atomic model following refinement against the cryo-EM map has excellent geometric parameters and comprises ~219,591 atoms (excluding hydrogens) across the 5,863 nucleotide residues and ~11,729 amino acids of the 80 proteins and the 4 rRNAs (28S, 5S, 5.8S and 18S; excluding certain expansion segments (ES) of rRNA, which are only partially visible at the periphery of the structure, probably owing to conformational heterogeneity). Furthermore, the atomic model includes 400 positions with Mg^{2+} ions in typical coordination environments, eight Zn^{2+} ions, 60 water molecules and two ligands (HYG and HTT). CHX is in a different atomic model that had a different ribosome conformation in the 3D classification, as the 80S–CHX complex was refined separately at a lower resolution and rRNA modifications are not resolved. The map contour level was adjusted to account for sub-stoichiometric ligand occupancy (Fig. 4). The atomic model contains 136 nucleotides and two amino acids with chemical modifications. Double conformations of side chains are seen on Arg70 of protein uL30 (providing alternative hydrogen bonds; Fig. 1b), Lys341 (protein uL3), Arg85 (protein eS26), Arg200 (protein uS5) and Arg138 (protein uS4). Protein residues show well-refined geometrical parameters (allowed regions 9.36%, preferred regions 90.38%, in Ramachandran plots and 0.26% outliers; Extended Data Table 1a). Figures were prepared using the Chimera[62] and PyMOL software (DeLano, 2006).

Analysis of molecular interactions involving rRNA modifications. The observed rRNA modification sites were classified into universally conserved locations (class I), human/eukaryote-specific modifications (class II) and new unpredicted unique sites (class III) (Extended Data Table 1b). Class I and II modifications also included some semi-conserved sites, such as m^{7}G4550 (28S rRNA), which is conserved as a modification site but altered differently because of a sequence change in this region (Ψ2605 in *E. coli*). The same holds for a set of Ψs: m^{3}Ψ1860, m^{1}Ψ3762 and m^{3}Ψ4296 (28S rRNA; Extended Data Fig. 7), which are methylated in the N3

position, and are not normal Ψs as databases would predict. $m^1Ψ3762$ (next to Ψ3764 at the tip of H69) is involved in bridge B2a through van der Waals contacts with Cm1710 in helix h44. The modified ac^4C1842 mentioned in the text contributes to inter-subunit bridge eB14 through an interaction with Arg2 in eL41 (eL41 connects the PTC and DC in 60S through modified nucleotides at its N and C termini; Fig. 3b). The structure shows that ac^4C1842 must be modified to interact with Arg2 at the subunit interface. The modifications may favour wobble base pairing in the rRNA, as occurs in DNA[37,38]. An example of this is a base triple in the vicinity of the modified $ac^7Gm3899$ and ac^7G3897 nucleotides: an acetyl moiety in the N7 position of ac^7G3897 extends the planarity of the base to create van der Waals contacts with the phosphate group of C3898 and the nucleotide base of A4559 (Fig. 5a). This stabilizes the neighbour non-classical C–A base interaction between C3896 and A4564 that shows a strong tilt angle (~45°), which propagates to the neighbour Watson–Crick base pair C4565–G3895 (Fig. 5b). Similarly, the modified m^6G4185 stabilizes the G–U pair (G4184 and U3927) and also stabilizes the rRNA loop, which harbours a flipped-out nucleotide (G4183; Fig. 5c). The methylation of m^5C3782 (Fig. 2g) is required for subunit stability[68,69] and introduces functional diversity in ribosomes, where m^5 methylation in C2278 in yeast leads to the recruitment of a specific subset of oxidative stress-responsive mRNAs into polyribosomes[70]. Some sites include inter-modification interactions, for example the modified A-minor contact $Am1678/m^3C1219$ (Fig. 3c) or the 2′-O-Me triplet in the H26/H47 multi-branch loop junction next to the PET, which increases the local packing between the RNA backbone and nucleotide bases (Fig. 2e). Finally, some chemical modifications disrupt the base planarity at the level of the attached moiety, for example the methylation in the C5 position of m^5C4447 or guanine modification in the N7 (for instance, in class III modifications: m^7G1605, xp^7G3880, m^2xp^7G4371 and m^7G4550) or O6 position (for instance, xp^6G1574, m^6G4185 and xe^6G4355) (Fig. 2c and Extended Data Fig. 8). In this context, it is remarkable to observe a series of nucleotides that are modified at the oxygen position, which is unusual for RNA (O6 in guanosine and O4 in uridine; for instance, xp^4U1348, xp^6G1574, xp^4U1659, xp^4U4194, m^6G4185 and xe^6G4355; Fig. 2c and Extended Data Fig. 8). Modifications at rRNA m^5C sites have functional implications, such as in translational fidelity and tRNA recognition[71]. For example, m^5C3782 forms a universally conserved tertiary stacking at the inter-subunit bridge B3 (Fig. 2g), and is crucial for subunit stability[68,69]. A similar modification at the PTC, m^5C4447, affects ribosome synthesis and processing[69].

HYG is located in proximity to Cm1703 (human-specific), m^3U1830, m^6A1832, $m^6{}_2A1850$ and $m^6{}_2A1851$ (18S rRNA; Fig. 4b). Consideration of these interactions, and comparison to the *E. coli* ribosome complex with HYG[54] could be used to create antibiotics with increased specificity. The interactions observed in the E site close to the CHX binding site suggest that rRNA modifications have a role in tRNA recognition at the E site. This hypothesis is supported by the presence of Ψ3715 and Am3718 (helix H68 in 28S rRNA), which are located near the tRNA acceptor stem of the E site (the phosphate backbone of Ψ3715 interacts with the ribose moieties of the tRNA bases C4 and A5). The additional group at the N2 position of m^2xp^7G4371 generates a hydrophobic contact with the glutarimide moiety of CHX in the vicinity of the 2′-O-methyl group of Gm4370 (Fig. 4c, d). Finally, several other known inhibitor binding pockets comprise modified nucleotides. For example, on the basis of modelling analysis based on the present structure of the human ribosome, blasticidin binds next to Cm3909 (60S), on the opposite face to HHT; geneticin and HYG share the same binding pocket containing $m^3Ψ1830$ (40S); like CHX, lactimidomycin and phyllanthoside bind next to Gm4370 and m^2xp^7G4371 (60S); and edeine would bind adjacent to the modified m^3U1830 and m^2A1832 in the mRNA channel.

Data availability. Atomic coordinates and the cryo-EM map have been deposited in the Protein Data Bank and EMDB under accession codes 6EK0 and EMD-3883, respectively. A 3D video of the human ribosome structure is available in the Supplementary Information and a high-resolution video is available at http://doi.org/10.6084/m9.figshare.5472523. All other materials are available upon reasonable request.

51. Khatter, H. *et al.* Purification, characterization and crystallization of the human 80S ribosome. *Nucleic Acids Res.* **42,** e49 (2014).
52. Garreau de Loubresse, N. *et al.* Structural basis for the inhibition of the eukaryotic ribosome. *Nature* **513,** 517–522 (2014).
53. Brodersen, D. E. *et al.* The structural basis for the action of the antibiotics tetracycline, pactamycin, and hygromycin B on the 30S ribosomal subunit. *Cell* **103,** 1143–1154 (2000).
54. Borovinskaya, M. A., Shoji, S., Fredrick, K. & Cate, J. H. D. Structural basis for hygromycin B inhibition of protein biosynthesis. *RNA* **14,** 1590–1599 (2008).
55. Gürel, G., Blaha, G., Moore, P. B. & Steitz, T. A. U2504 determines the species specificity of the A-site cleft antibiotics: the structures of tiamulin, homoharringtonine, and bruceantin bound to the ribosome. *J. Mol. Biol.* **389,** 146–156 (2009).
56. Zheng, S. Q. *et al.* MotionCor2: anisotropic correction of beam-induced motion for improved cryo-electron microscopy. *Nat. Methods* **14,** 331–332 (2017).
57. Zhang, K. Gctf: Real-time CTF determination and correction. *J. Struct. Biol.* **193,** 1–12 (2016).
58. Scheres, S. H. W. RELION: implementation of a Bayesian approach to cryo-EM structure determination. *J. Struct. Biol.* **180,** 519–530 (2012).
59. Chen, S. *et al.* High-resolution noise substitution to measure overfitting and validate resolution in 3D structure determination by single particle electron cryomicroscopy. *Ultramicroscopy* **135,** 24–35 (2013).
60. Rosenthal, P. B. & Henderson, R. Optimal determination of particle orientation, absolute hand, and contrast loss in single-particle electron cryomicroscopy. *J. Mol. Biol.* **333,** 721–745 (2003).
61. Kucukelbir, A., Sigworth, F. J. & Tagare, H. D. Quantifying the local resolution of cryo-EM density maps. *Nat. Methods* **11,** 63–65 (2014).
62. Pettersen, E. F. *et al.* UCSF Chimera—a visualization system for exploratory research and analysis. *J. Comput. Chem.* **25,** 1605–1612 (2004).
63. Emsley, P., Lohkamp, B., Scott, W. G. & Cowtan, K. Features and development of Coot. *Acta Crystallogr. D Biol. Crystallogr.* **66,** 486–501 (2010).
64. Natchiar, K. S., Myasnikov, A. G., Kratzat, H., Hazemann, I. & Klaholz, B. P. Atomic model building and refinement into high-resolution cryo-EM maps. *Protocol Exchange* http://dx.doi.org/10.1038/protex.2017.122 (2017).
65. Afonine, P. V. *et al.* Towards automated crystallographic structure refinement with phenix.refine. *Acta Crystallogr. D Biol. Crystallogr.* **68,** 352–367 (2012).
66. Lebedev, A. A. *et al.* JLigand: a graphical tool for the CCP4 template-restraint library. *Acta Crystallogr. D Biol. Crystallogr.* **68,** 431–440 (2012).
67. Yang, H., Henning, D. & Valdez, B. C. Functional interaction between RNA helicase II/Guα and ribosomal protein L4. *FEBS J.* **272,** 3788–3802 (2005).
68. Gigova, A., Duggimpudi, S., Pollex, T., Schaefer, M. & Koš, M. A cluster of methylations in the domain IV of 25S rRNA is required for ribosome stability. *RNA* **20,** 1632–1644 (2014).
69. Sharma, S., Yang, J., Watzinger, P., Kötter, P. & Entian, K.-D. Yeast Nop2 and Rcm1 methylate C2870 and C2278 of the 25S rRNA, respectively. *Nucleic Acids Res.* **41,** 9062–9076 (2013).
70. Schosserer, M. *et al.* Methylation of ribosomal RNA by NSUN5 is a conserved mechanism modulating organismal lifespan. *Nat. Commun.* **6,** 6158 (2015).
71. Chow, C. S., Lamichhane, T. N. & Mahto, S. K. Expanding the nucleotide repertoire of the ribosome with post-transcriptional modifications. *ACS Chem. Biol.* **2,** 610–619 (2007).

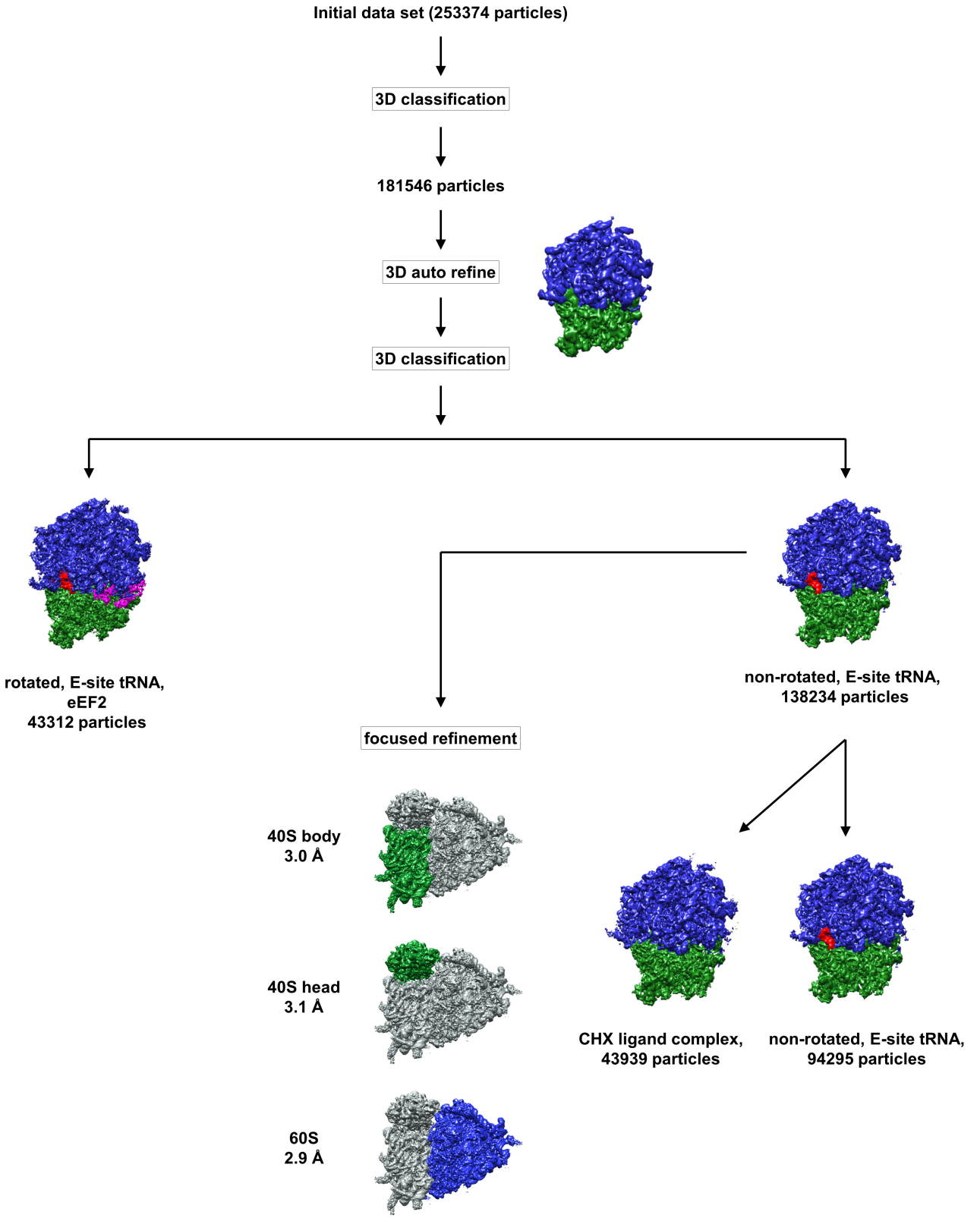

Extended Data Figure 1 | Particle sorting scheme. The initial dataset (top) was sorted into two main 3D classes (+/− rotated) and particles of the non-rotated state were either split further, depending on whether tRNA is bound to the E site (absence of tRNA means CHX is bound), or subjected to focused refinement of the 60S subunit and the 40S subunit head and body parts.

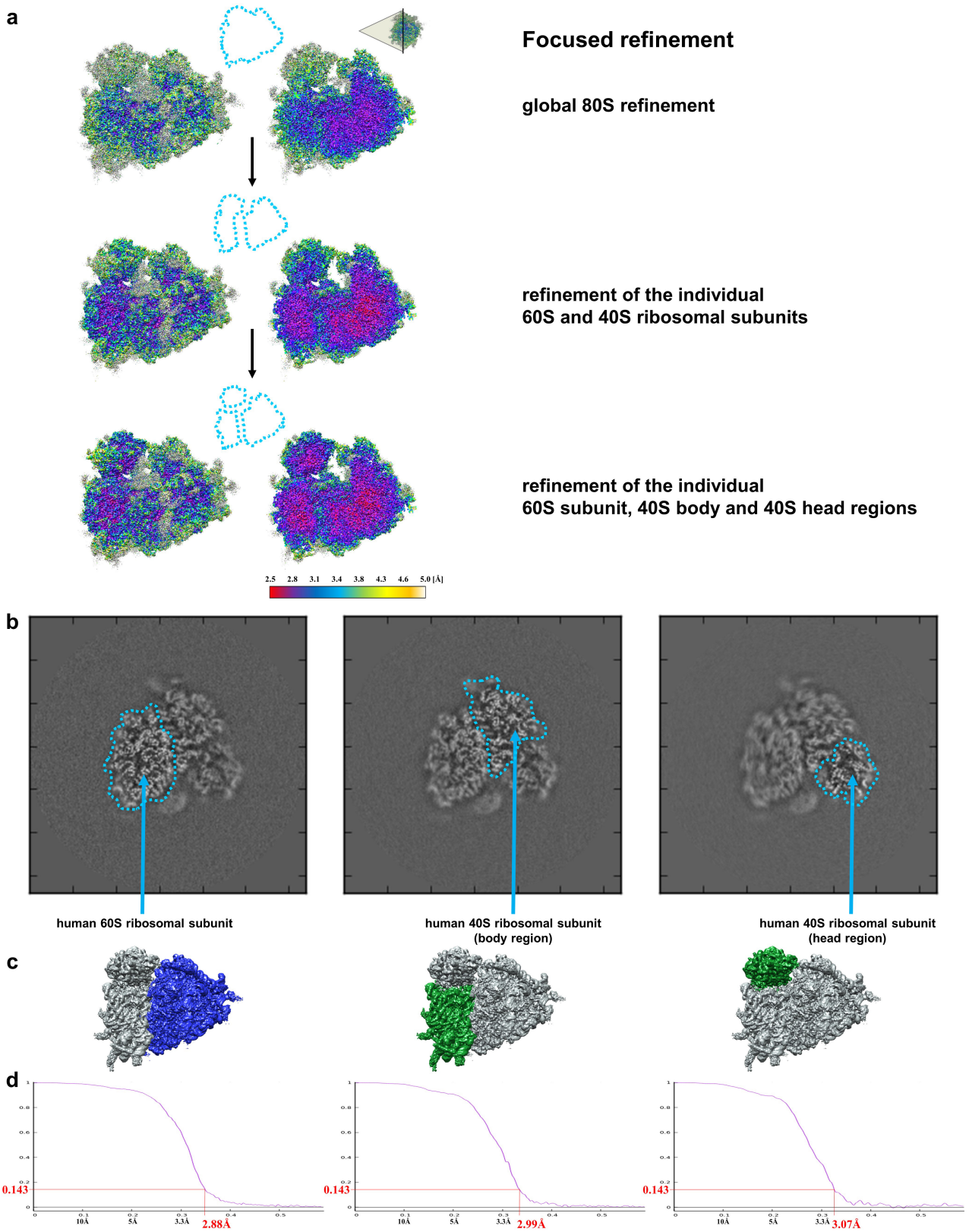

Extended Data Figure 2 | Focused refinement and resolution estimation. a, Focused refinement of the 60S subunit and the 40S subunit head and body regions (left, entire 80S complex; right, central section). **b**, Sections through the individually refined regions during focused refinement (the individually refined areas are sharp, whereas the other regions are less ordered). **c**, Individually refined regions in the 80S structure. **d**, Resolution estimation from the FSC curves.

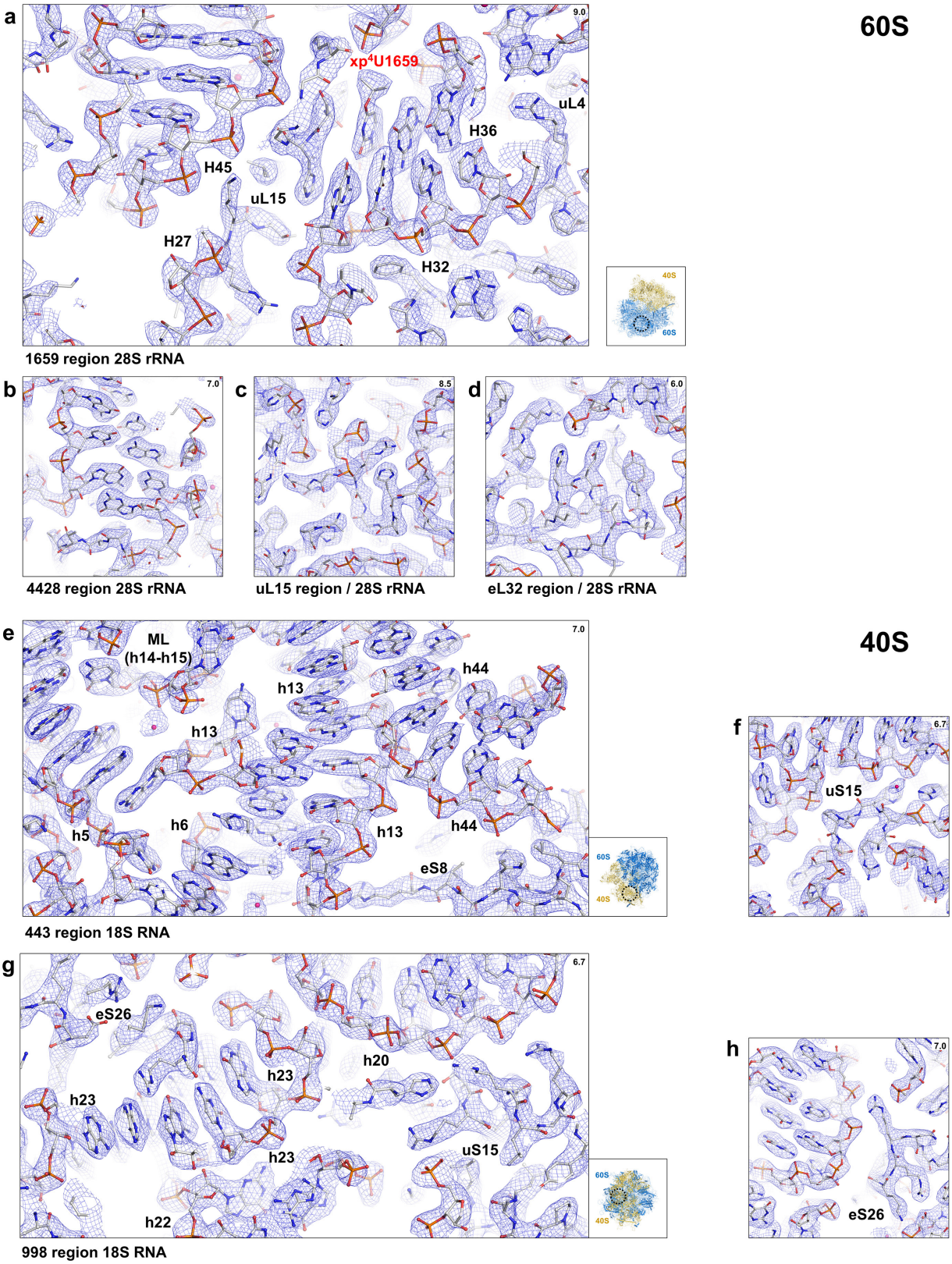

Extended Data Figure 3 | Representative regions in the 60S and 40S ribosomal subunits. a–d, Cryo-EM map and atomic model of various regions in the 60S subunit. **e–h**, Cryo-EM map and atomic model of various regions in the 40S subunit.

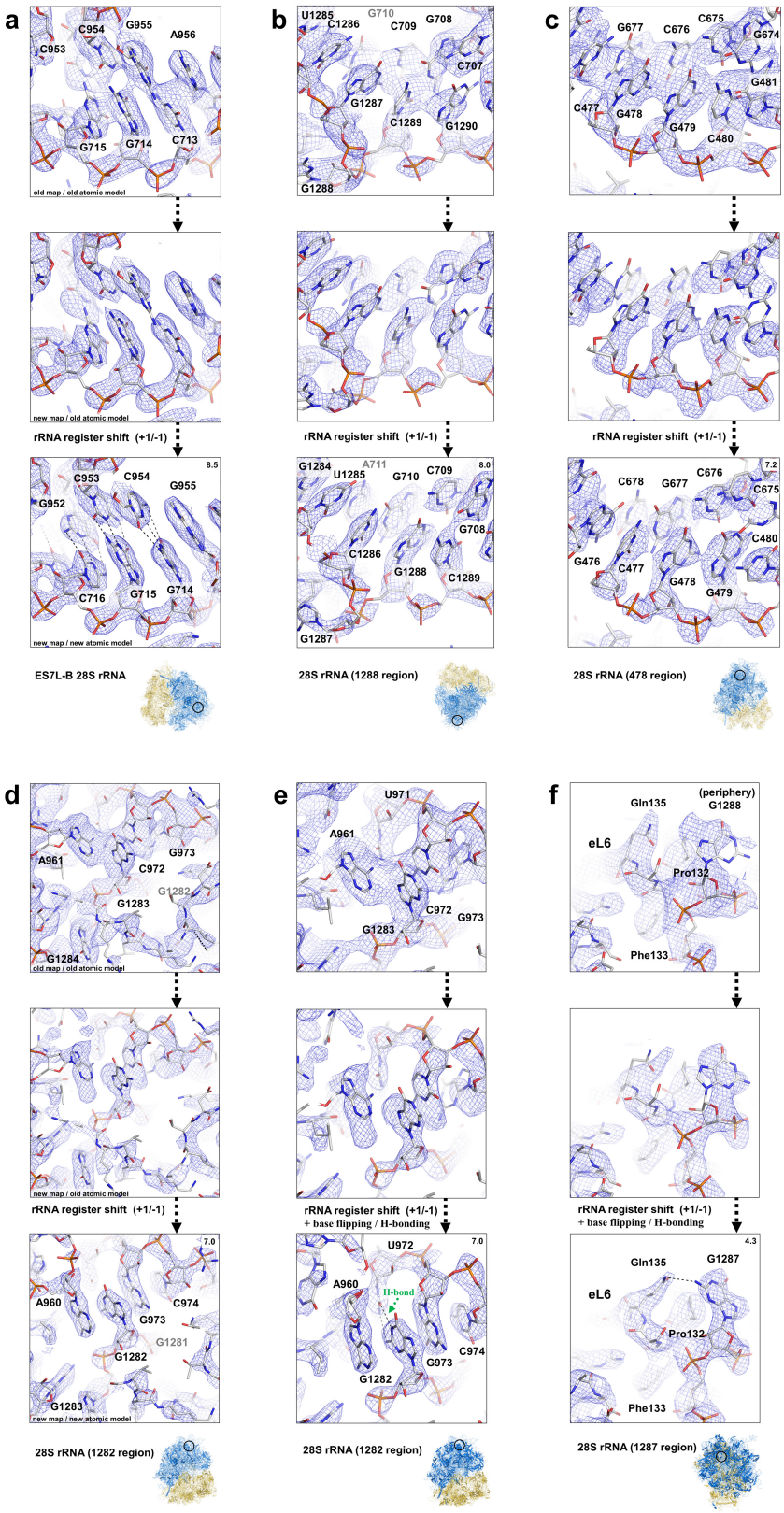

Extended Data Figure 4 | Register shift examples in previously less ordered rRNA regions. a–f, Comparison of the previous map and previous atomic model[23] (top), with the new map and the previous model (middle), and the new map with the refined atomic model after correction of register shifts.

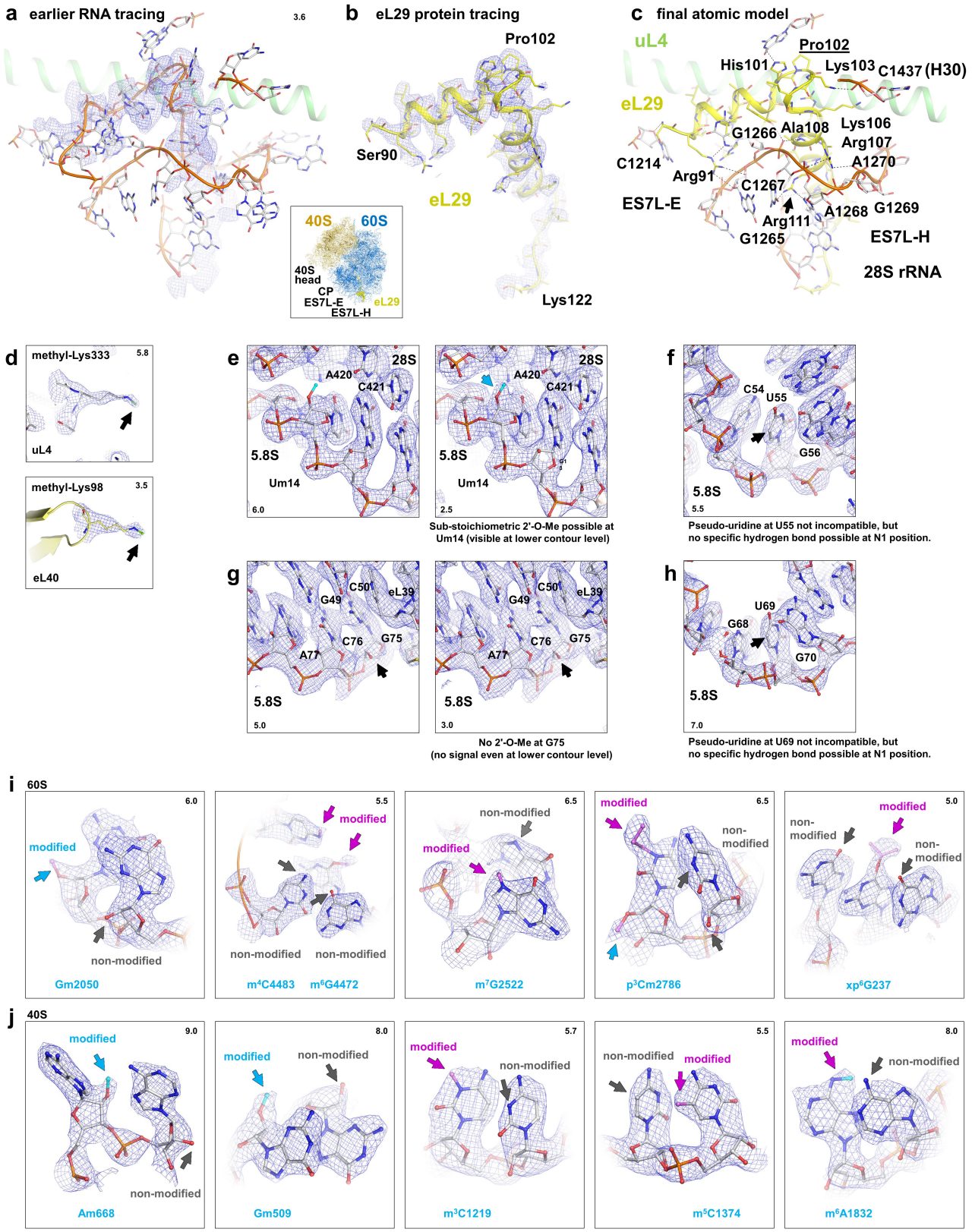

Extended Data Figure 5 | Specific features in the human ribosome structure. a–c, Reannotation of an rRNA region as a ribosomal protein (eL29). **d**, Protein modifications on two lysine residues. **e–h**, Analysis of rRNA modifications in the 5.8S rRNA including sub-stoichiometric modification of Um14. **i**, **j**, Comparisons of neighbouring residues with and without rRNA modifications (human 60S and 40S ribosomal subunits, respectively).

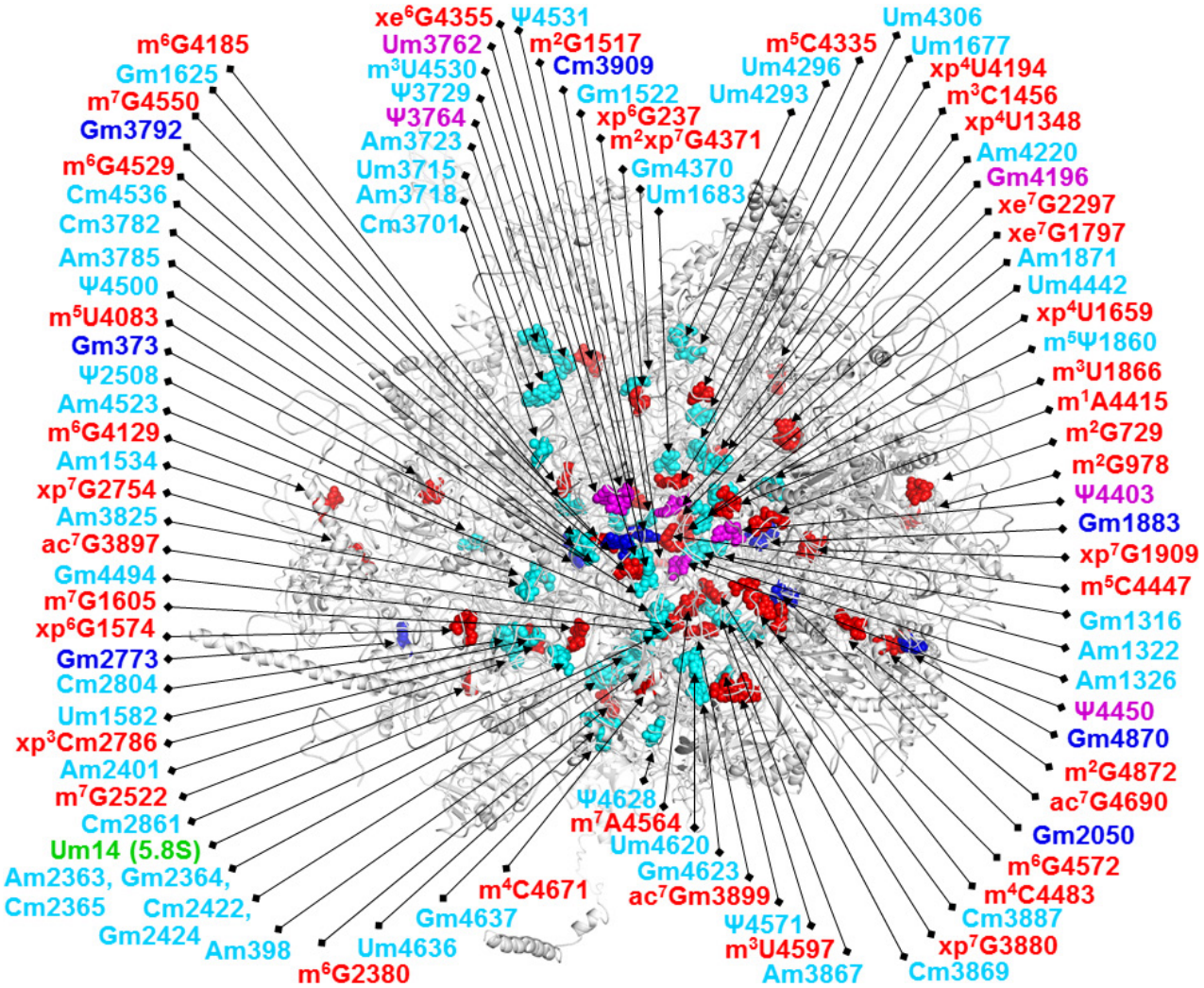

Extended Data Figure 6 | Annotation of chemical modifications in the 60S ribosomal subunit. Conserved sites in *E. coli* and human large ribosomal subunits (magenta), predicted and found sites (cyan), unpredicted 2′-O-Me modification sites (blue), unpredicted base modification sites (red) and a 5.8S rRNA modification (green).

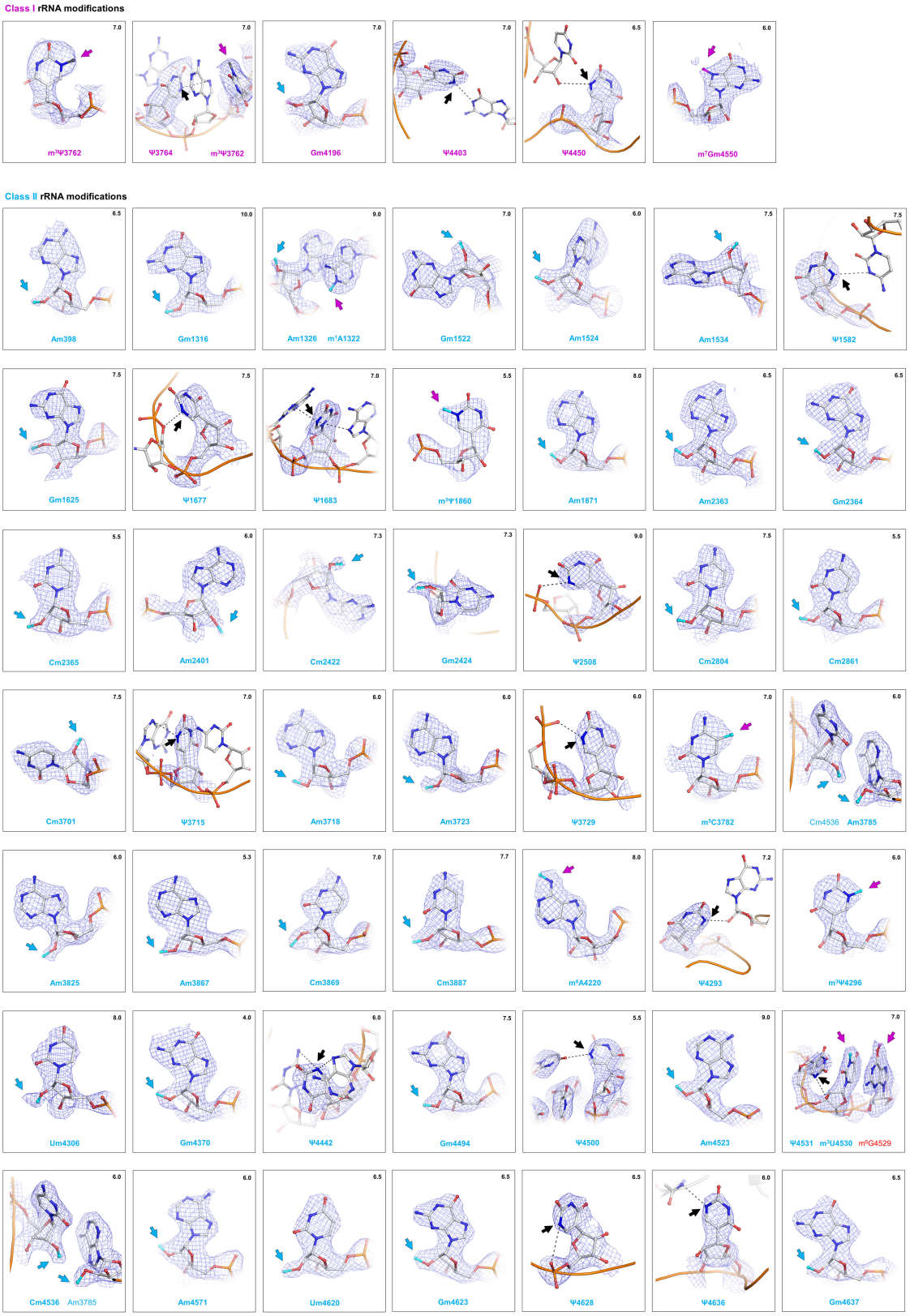

Extended Data Figure 7 | Detailed views of the chemical modifications in the 60S ribosomal subunit (class I and class II). Individual modification sites in classes I and II (magenta and cyan, respectively; cyan arrows indicate 2′-O-ribose methylations, black arrows indicate Ψs validated through the specific hydrogen-bond pattern, other modifications are indicated with magenta arrows).

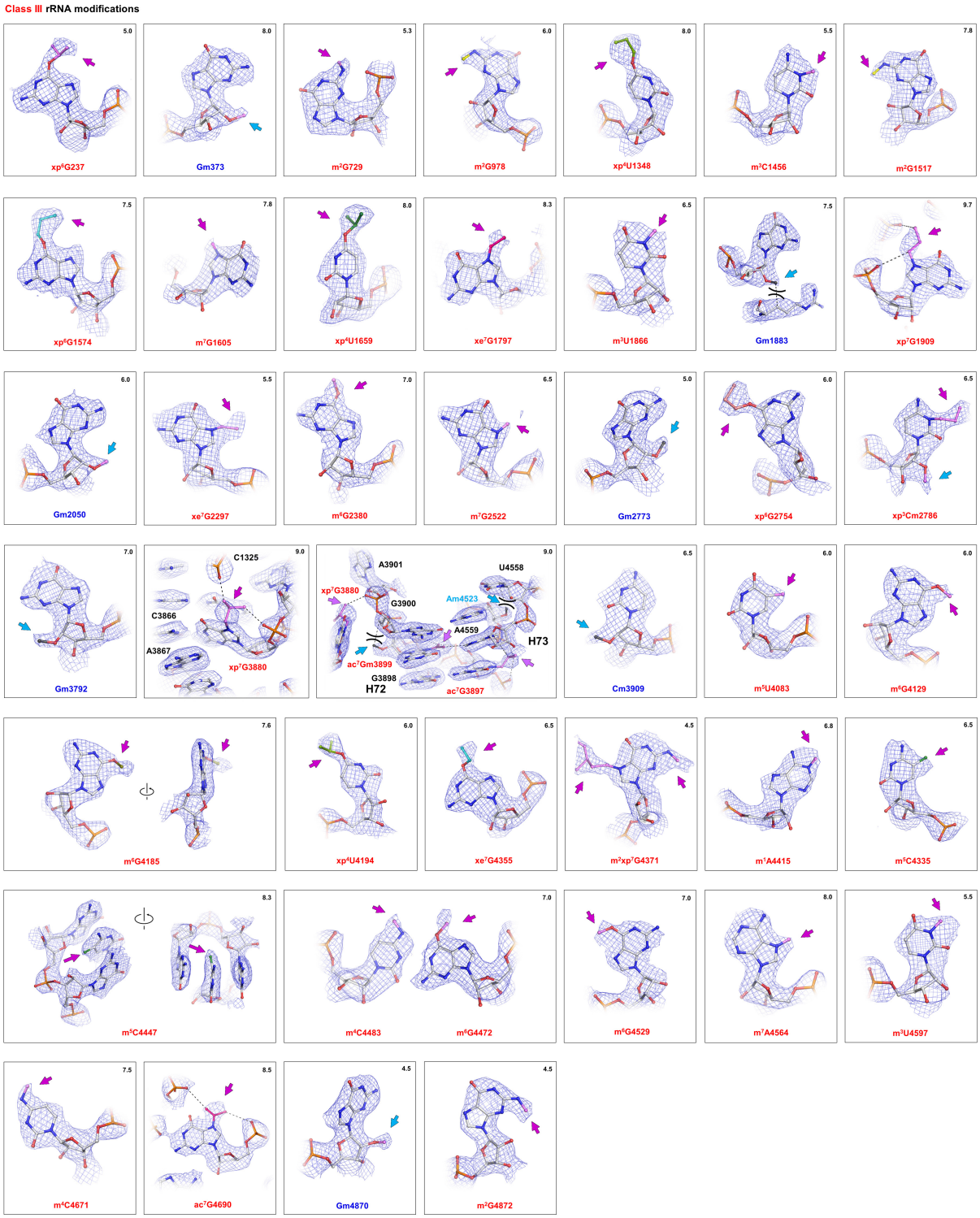

Extended Data Figure 8 | Detailed views of the chemical modifications in the 60S ribosomal subunit (class III). Individual modification sites in class III (red; arrow colours as in Extended Data Fig. 7).

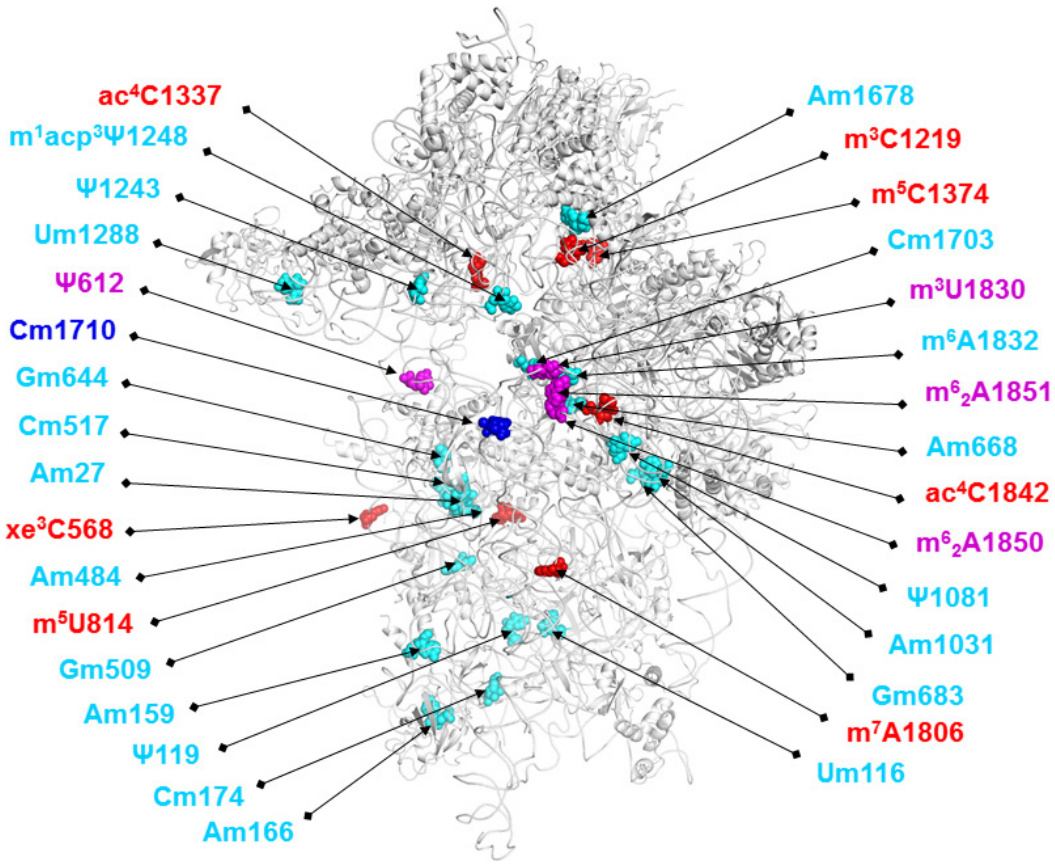

Extended Data Figure 9 | Annotation of chemical modifications in the 40S ribosomal subunit. Conserved sites in *E. coli* and human (magenta), predicted and found sites (cyan), unpredicted 2′-O-Me modification sites (blue) and unpredicted base modification sites (red).

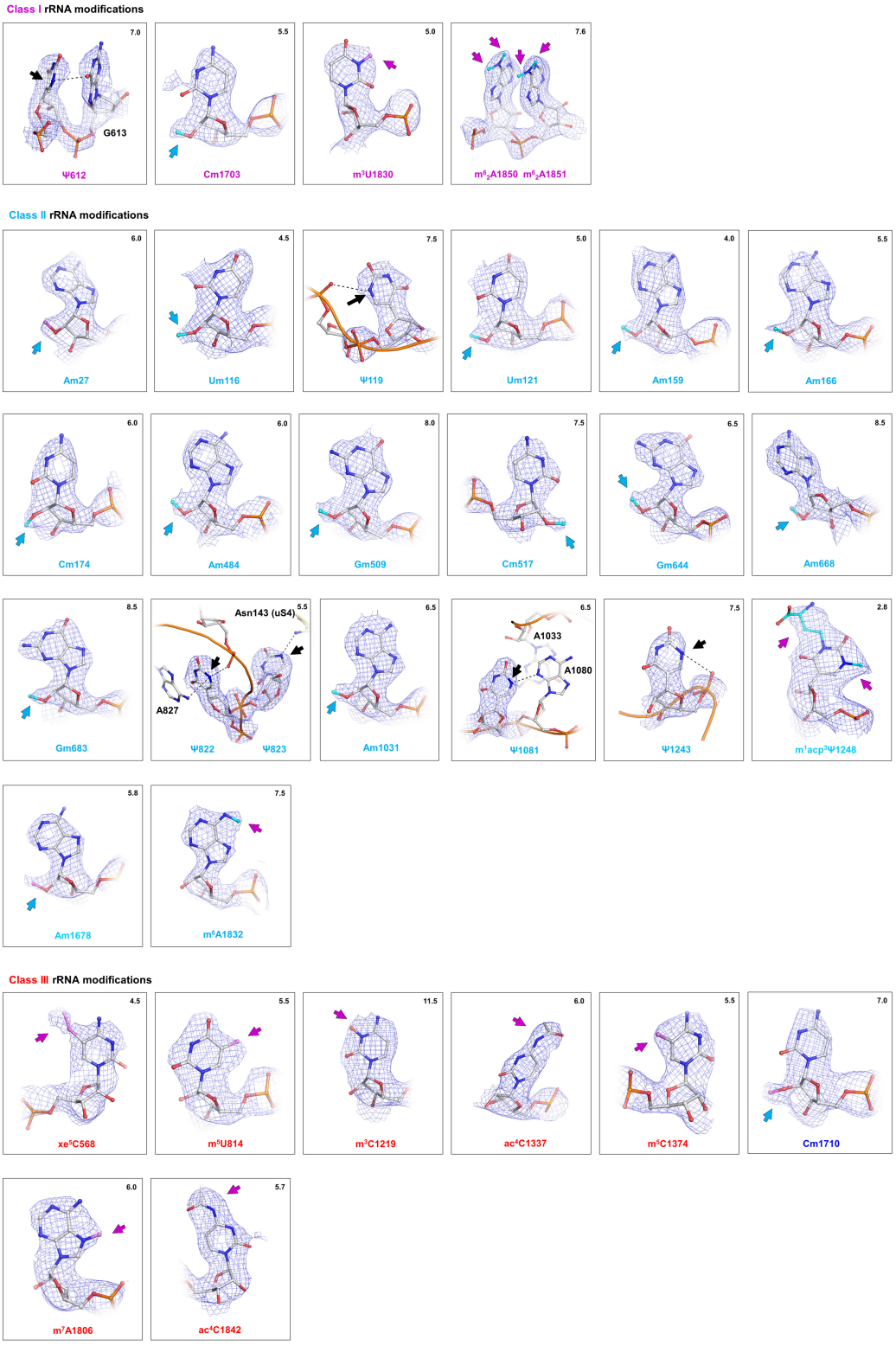

Extended Data Figure 10 | Detailed views of the chemical modifications in the 40S ribosomal subunit (classes I, II and III). Individual modification sites in classes I, II and III (in magenta, cyan and red, respectively; arrow colours as in Extended Data Fig. 7).

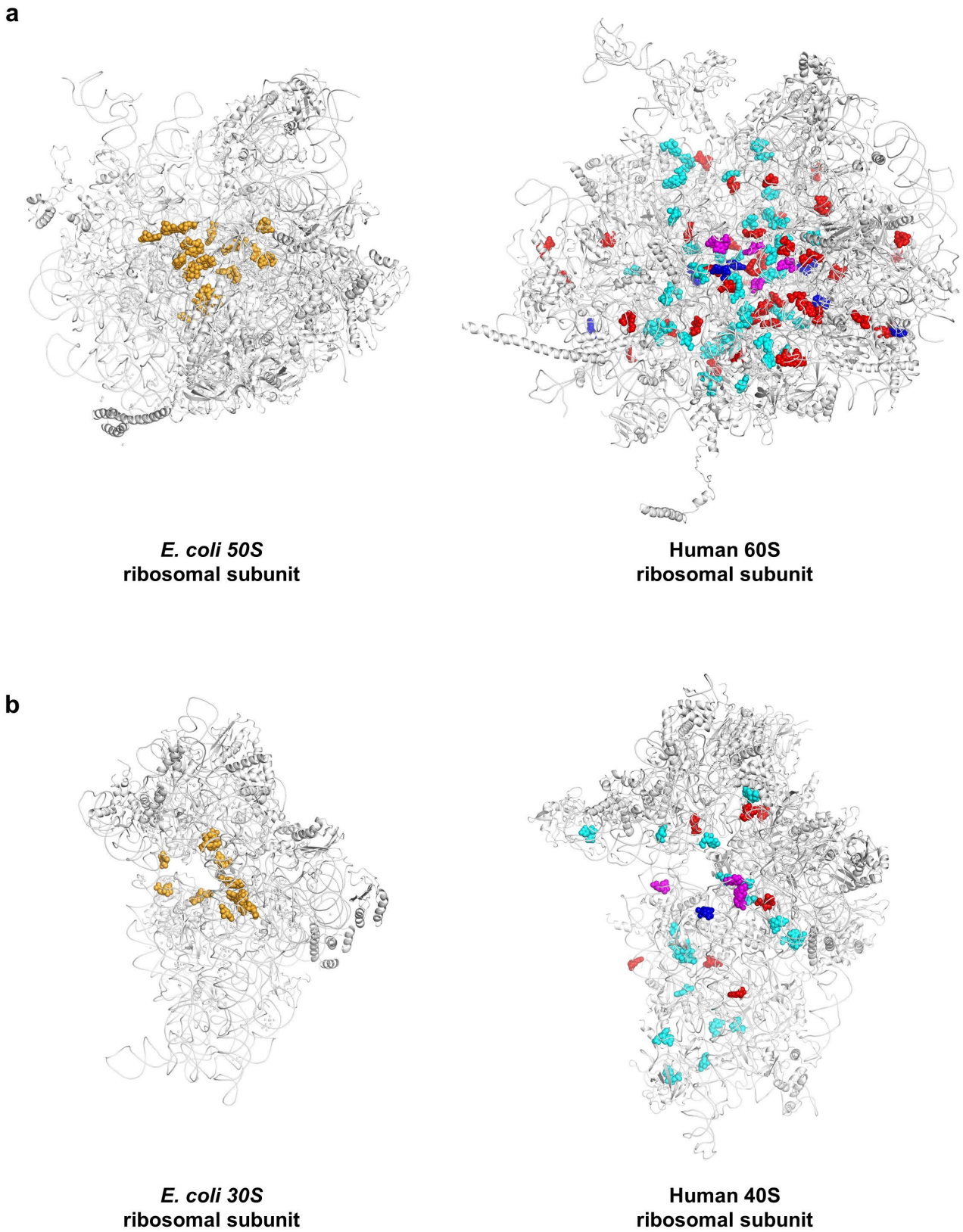

Extended Data Figure 11 | rRNA modifications in *E. coli* and human ribosomal subunits. a, Large ribosomal subunit (left, *E. coli*; right, human). **b**, Small ribosomal subunit (left, *E. coli*; right, human).

Extended Data Table 1 | Data, statistics and classification of rRNA modifications

a

Data Collection	
Particles	139,234
Sampling (Å/pixel)	0.85
Defocus range (μm)	-0.4 to -2.5
Atomic model composition	
Non-hydrogen atoms	219,591
Amino acids	11,729
Nucleotides	5,863
Number of ligand atoms	75
Zn^{2+} / Mg^{2+} / H_2O	8 / 400 / 60
Refinement	
Average resolution (Å)	2.9 (60S) / 3.0 (40S body) / 3.1 (40S head)
Average B-factor ($Å^2$)	64.4
RMS Deviation	
Bond lengths (Å)	0.009
Bond angles (°)	1.057
Ramachandran statistics	
Favoured (%)	90.38
Allowed (%)	9.36
Outliers (%)	0.26

b

	2'-O-Me & 2'-O-Me with base modifications	**Base modifications**	**Ψ**	**Ψ with other base modifications**	**Total**
Class I	2	4	4	1	11
Class II	48	5	17	3	73
Class III	8+2	42	-	-	52
Total	60	51	21	4	136

a, Table containing data collection and atomic model refinement statistics. **b**, Number of rRNA modifications in each class.

nature research

Corresponding author(s): Bruno Klaholz

☐ Initial submission ☐ Revised version ☒ Final submission

Life Sciences Reporting Summary

Nature Research wishes to improve the reproducibility of the work that we publish. This form is intended for publication with all accepted life science papers and provides structure for consistency and transparency in reporting. Every life science submission will use this form; some list items might not apply to an individual manuscript, but all fields must be completed for clarity.

For further information on the points included in this form, see Reporting Life Sciences Research. For further information on Nature Research policies, including our data availability policy, see Authors & Referees and the Editorial Policy Checklist.

Experimental design

1. Sample size

   Describe how sample size was determined. N/A

2. Data exclusions

   Describe any data exclusions. N/A

3. Replication

   Describe whether the experimental findings were reliably reproduced. N/A

4. Randomization

   Describe how samples/organisms/participants were allocated into experimental groups. N/A

5. Blinding

   Describe whether the investigators were blinded to group allocation during data collection and/or analysis. N/A

   Note: all studies involving animals and/or human research participants must disclose whether blinding and randomization were used.

6. Statistical parameters

   For all figures and tables that use statistical methods, confirm that the following items are present in relevant figure legends (or in the Methods section if additional space is needed).

n/a	Confirmed
☒	☐ The exact sample size (*n*) for each experimental group/condition, given as a discrete number and unit of measurement (animals, litters, cultures, etc.)
☒	☐ A description of how samples were collected, noting whether measurements were taken from distinct samples or whether the same sample was measured repeatedly
☒	☐ A statement indicating how many times each experiment was replicated
☒	☐ The statistical test(s) used and whether they are one- or two-sided (note: only common tests should be described solely by name; more complex techniques should be described in the Methods section)
☒	☐ A description of any assumptions or corrections, such as an adjustment for multiple comparisons
☒	☐ The test results (e.g. *P* values) given as exact values whenever possible and with confidence intervals noted
☒	☐ A clear description of statistics including central tendency (e.g. median, mean) and variation (e.g. standard deviation, interquartile range)
☒	☐ Clearly defined error bars

See the web collection on statistics for biologists for further resources and guidance.

Software

Policy information about availability of computer code

7. Software

Describe the software used to analyze the data in this study.	Cryo-EM image processing software (academic softwares such as Relion, Imagic, EMAN)

For manuscripts utilizing custom algorithms or software that are central to the paper but not yet described in the published literature, software must be made available to editors and reviewers upon request. We strongly encourage code deposition in a community repository (e.g. GitHub). *Nature Methods* guidance for providing algorithms and software for publication provides further information on this topic.

Materials and reagents

Policy information about availability of materials

8. Materials availability

Indicate whether there are restrictions on availability of unique materials or if these materials are only available for distribution by a for-profit company.	N/A

9. Antibodies

Describe the antibodies used and how they were validated for use in the system under study (i.e. assay and species).	N/A

10. Eukaryotic cell lines

a. State the source of each eukaryotic cell line used.	HeLa cell line
b. Describe the method of cell line authentication used.	HeLa cells were tested by polymerase chain reaction for Mycoplasma and certified as free of Mycoplasma.
c. Report whether the cell lines were tested for mycoplasma contamination.	N/A
d. If any of the cell lines used are listed in the database of commonly misidentified cell lines maintained by ICLAC, provide a scientific rationale for their use.	N/A

Animals and human research participants

Policy information about studies involving animals; when reporting animal research, follow the ARRIVE guidelines

11. Description of research animals

Provide details on animals and/or animal-derived materials used in the study.	N/A

Policy information about studies involving human research participants

12. Description of human research participants

Describe the covariate-relevant population characteristics of the human research participants.	N/A